Induction of apoptosis in ovarian cancer cells by miR-493-3p directly targeting AKT2, STK38L, HMGA2, ETS1 and E2F5

Michael Kleemann[1,2,*], Helga Schneider[1], Kristian Unger[3], Jeremias Bereuther[4], Simon Fischer[5], Philip Sander[6], E. Marion Schneider[6], Pamela Fischer-Posovszky[7], Christian U. Riedel[8], René Handrick[1], Kerstin Otte[1]

[1] Institute of Applied Biotechnology, University of Applied Sciences Biberach, Hubertus-Liebrecht-Str. 35, 88400 Biberach, Germany

[2] University of Ulm, Faculty of Medicine, Albert-Einstein-Allee 11, 89079 Ulm, Germany

[3] Research Unit Radiation Cytogenetics, Helmholtz Zentrum München Helmholtz Center Munich, German Research Center for Environmental Health, Ingolstädter Landstr. 1, 85764 Neuherberg, Germany

[4] apceth Biopharma GmbH, Haidgraben 5, 85521 Ottobrunn, Germany

[5] Boehringer Ingelheim Pharma GmbH & Co. KG, Bioprocess and Analytical Development, Birkendorfer Straße 65, 88400 Biberach, Germany

[6] University Medical Center Ulm, Division of Experimental Anesthesiology, Albert-Einstein-Allee 23, 89081 Ulm, Germany

[7] University Medical Center Ulm, Division of Pediatric Endocrinology and Diabetes, Department of Pediatrics and Adolescent Medicine, Eythstr. 24, 89075 Ulm, Germany

[8] University of Ulm, Faculty of Medicine, Albert-Einstein-Alee 11, 89081 Ulm, Germany

[*]: Corresponding author: Michael Kleemann

E-Mail: kleemann@hochschule-bc.de

Phone: +49 (0) 7351 582-455

Fax: +49 (0) 7351 582-469
Postal address: Institute of Applied Biotechnology
University of Applied Sciences Biberach
Hubertus-Liebrecht-Str. 35
88400 Biberach, Germany

Acknowledgement

This study was funded by the Postgraduate Scholarships Act of the Ministry for Science, Research and Arts of the Federal State Government of Baden-Wuerttemberg, Germany. Further acknowledgements address the International Graduate School in Molecular Medicine of Ulm University, Germany, for scientific encouragement and support to Michael Kleemann.

Pamela Fischer-Posovszky receives funding from the Baden-Württemberg Stiftung, Germany.

The results published here are based upon data generated by the TCGA Research Network.

In addition, the authors are grateful to Dr. Anne-Marie Mes-Masson (Centre Hospitalier de l´Université de Montréal, Canada) for providing us with the TOV21G and TOV112D cells as well as to Alex Shu-Wing Ng (Department of Obstetrics, Gynecology and Reproductive Biology, the Brigham and Women's Hospital, Boston, USA) for the HOSE 2170 cells. The OVCAR3, A2780 and A2780-cis cells were kindly provided by Verena Jendrossek (Institute of Cell Biology (Cancer Research), University of Duisburg-Essen, Germany).

Keywords

microRNA, cancer, signalling pathways, targets, RAF1

Abstract

Apoptosis is a form of directed programmed cell death with a tightly regulated signalling cascade for the destruction of single cells. MicroRNAs (miRNAs) play an important role as fine tuners in the regulation of apoptotic processes. MiR-493-3p mimic transfection leads to the induction of apoptosis causing the breakdown of mitochondrial membrane potential and the activation of caspases resulting in the fragmentation of DNA in several ovarian carcinoma cell lines. Ovarian cancer shows with its pronounced heterogeneity a very high death-to-incidence ratio. A target gene analysis for miR-493-3p was performed for the investigation of underlying molecular mechanisms involved in apoptosis signalling pathways. Elevated miR-493-3p levels downregulated the mRNA and protein expression levels of Serine/Threonine Kinase 38 Like (STK38L), High Mobility Group AT-Hook 2 (HMGA2) and AKT Serine/Threonine Kinase 2 (AKT2) by direct binding as demonstrated by luciferase reporter assays. Notably, the protein expression of RAF1 Proto-Oncogene, Serine/Threonine Kinase (RAF1) was almost completely downregulated by miR-493-3p. This interaction, however, was indirect and regulated by STK38L phosphorylation. In addition, RAF1 transcription was diminished as a result of reduced transcription of ETS proto-oncogene 1 (ETS1), another direct target of miR-493. Taken together, our observations have uncovered the apoptosis inducing potential of miR-493-3p through its regulation of multiple target genes participating in the extrinsic and intrinsic apoptosis pathway.

Introduction

Apoptosis is a form of directed programmed cell death for the destruction of only single cells without damaging surrounding tissues [1]. It is induced via two distinct but interrelated main signalling pathways, an intrinsic and an extrinsic one. The extrinsic pathway is initiated by ligand binding to a transmembrane receptor (i.e. via the tumour necrosis factor receptor (TNFR) [1]) or the vascular endothelial growth factor receptor (VEGFR) leading to the regulation of the mitogen-activated protein kinase / extracellular signal-regulated kinase (MAPK/ERK) signalling pathway [2]. The intrinsic pathway is induced by the release of cytochrome C from the mitochondria and involves different non-receptor-mediated stimuli. The integrity of the mitochondria is mediated by different pro- and anti-apoptotic B-cell lymphoma 2 (Bcl2) members such as Bcl-2-associated X protein (Bax) and Bcl-2 homologous antagonist killer (Bak) [3]. The release of cytochrome C activates the initiator caspase 9, leading to the activation of effector caspase 3 [3]. Caspase 3 is furthermore cleaving and thereby inactivating the DNA repair protein poly (ADP-ribose) polymerase (PARP) [4]. Finally, genomic DNA is cleaved by caspase-activated deoxyribonucleases [5]. Apoptosis represents a tightly regulated signalling cascade culminating in activation of caspases and subsequent specific morphological and biochemical changes resulting in the elimination of degenerated cells by phagocytosis [1].

Previous studies showed that microRNAs (miRNAs) play an important role as fine tuners in the regulation of physiological and pathological cellular processes such as apoptosis, proliferation or differentiation [6] [7]. MiRNAs are endogenous single-stranded small non-coding RNAs with a length of around 22 nucleotides [8]. They are transcribed by RNA-polymerase II and processed by the RNase-III enzymes DROSHA and DICER. The processed miRNAs are bound to Argonaut 2 proteins and guided to the RNA induced silencing complex. The miRNA guide strand can bind to

the 3 prime untranslated region (3' UTR) of a target gene and thereby functions as post-transcriptional regulator [9]. With the imperfect base pairing of the miRNA to the target mRNA, one miRNA can target multiple genes and therefore interact in several signalling pathways [7]. Binding of a miRNA to the target mRNA typically leads to translational repression or mRNA decay by endonucleolytical cleavage [9].

Several miRNAs have already been reported to play a role in the regulation of apoptotic signalling pathways for example by targeting the mRNA of Bcl2 proteins, caspases or members of the p53 network [10] [11]. This may lead to cancer development or treatment resistance [12]. The identification of death inducing miRNAs might influence the outcome of treatment therapies [13], overcome treatment resistances and help to cure cancer (CA).

Ovarian CA is a common human CA with poor prognosis and the highest death-to-incidence ratio. For 2017, the American Cancer Society estimates 22,440 new cases and 14,080 deaths due to ovarian CA in the United States [14]. Ovarian CA refers to a highly heterogeneous type of CA including the subgroup epithelial ovarian carcinoma [15]. Patients are treated with chemotherapy i.e. with Carboplatin and Paclitaxel for 3 to 6 cycles [16]. However, due to the often arising resistances researchers are focusing on oncogenes as well as cell signalling pathways exploring their role in tumour progression [17] to overcome these obstacles. As miRNAs target multiple genes and signalling pathways [7] they are highly interesting molecules for the generation of novel anticancer therapeutics. However, signalling pathways involved in miRNA mediated apoptosis need to be further investigated.

Based on a previous cellular high throughput screening [18] we identified miR-493-3p to strongly induce apoptosis in the ovarian CA cell line SKOV3. The aim of this study was to identify the role of miR-493-3p in programmed cell death signalling of various ovarian CA cell lines. In particular, target genes regulated by miR-493-3p resulting in

altered signalling pathways that lead to cellular responses of cell death were investigated.

Results

Apoptosis screening identifies miR-493-3p as a novel pro-apoptotic miRNA in ovarian carcinoma cells

MicroRNAs are increasingly gaining interest as tumour suppressor-genes with their potential to regulate important cellular processes such as apoptosis [19]. To identify novel pro-apoptotic miRNAs, we previously transfected 188 potential pro-apoptotic miRNA mimics into the human CA cell lines SKOV3, HCT 116 and T98G as well as in the preadipocytes SGBS and measured hallmarks of apoptosis induction by quantitative flow cytometry [18]. In the current study, we focused on miRNA-493-3p, which we found to induce significant apoptosis in SKOV3 cells (5.4 fold ± 0.5 fold increase compared to NT) as well as in HCT 116 cells (3.2 fold ± 0.4 fold increase compared to NT; Fig 1 a). The previously described pro-apoptotic miR-183-5p [20] induced apoptosis up to 6.6 fold ± 0.5 fold in SKOV3 cells compared to a non-targeting control (NT). As miR-493-3p showed the highest fold changes in the ovarian CA cell line SKOV3, we further investigated the influence of this miRNA in various ovarian CA cell lines.

Apoptosis induction increases aberrant miR-493-3p expression

MicroRNA-493 is known as a tumour suppressor in lung CA [21], human bladder CA [22] and gastric CA [23]. It is encoded on the human chromosome 14 (14q32) in the Delta Like Non-Canonical Notch Ligand 1 (DLK1) - Deiodinase, Iodothyronine Type III (DIO3) genomic region in an pattern of imprinted genes, long noncoding RNAs like maternally expressed 3 (Meg3) and Meg8 and several miRNAs [24] [25] (Fig 1 b).

In order to further assess the functions of miR-493 in the regulation of apoptosis in ovarian CA, the expression of miR-493 was examined in six different ovarian CA cell lines, SKOV3, OVCAR3, TOV21G, TOV112D, A2780 and A2780-cis (Cisplatin

resistant cells). Comparing the expression of both miRNA strands to normal human ovarian surface epithelial cells (HOSE 2170 cells) [26], the expression of the 3p and 5p strand of hsa-miR-493 was reduced to at least 0.03 fold ± 0.001 fold in TOV21G cells (Fig 1 c). After induction of apoptosis by treating the cells for 48 h with the clinically relevant chemotherapeutic drugs Carboplatin, Paclitaxel [16] and Etoposide as positive controls, the expression of hsa-miR-493 increased for both strands in both cell lines SKOV3 (Fig 1 d) and OVCAR3 (Fig 1 e). In general, the previously as potentially pro-apoptotic identified 3p strand of hsa-miR-493 was more consistently and higher induced by pro-apoptotic stimuli than the 5p strand, again suggesting an involvement in the initiation or progression of the apoptotic pathway.

MiR-493 induces apoptosis in ovarian carcinoma cells

To investigate the apoptotic effect of hsa-miR-493-3p in more detail, miR-493-3p mimic or a non-targeting control (NT) were individually transfected into ovarian CA cell lines. To verify elevated intracellular levels of the miRNAs after transfection, the amounts were assessed via qPCR revealing an increase of miR-493-3p by 3400 fold in SKOV3 or 6000 fold in OVCAR3 cells when compared to NT transfected cells (Supplementary Figure 1), confirming a generally high enrichment after transfection. Several methods were applied for the detection of various apoptosis stages to a panel of ovarian carcinoma cell lines with different genetic background including SKOV3^{p53null}, OVCAR3^{p53R248Q} [27], TOV21G, TOV112D^{p53R175H} [28], A2780 and A2780-cis^{p53K351N} [29] [30]. Regarding cell growth, hsa-miR-493-3p led to a significant reduction of cell confluence in the different ovarian cell lines. The highest reduction in cell confluence was detected in hsa-miR-493-3p transfected A2780 cells when compared to NT transfected cells (39.9 % ± 0.8 % vs 68.5 % ± 0.3 % cell confluence, respectively). The chemotherapeutic drugs Paclitaxel, Carboplatin and Etoposide as

well as the death inducing siRNA control (DT) were applied as controls known to reduce cell confluence after treatment (Fig 2 a). As cytochrome C is released from the mitochondria into the cytoplasm after induction of apoptosis, its release as well as alterations in mitochondrial membrane potential (ΔΨm) were analysed by flow cytometry employing the potential-sensitive fluorescent dye tetramethylrhodamine ethyl ester (TMRE). Comparing the different ovarian CA cell lines, the highest release of cytochrome C was detected in miR-493-3p transfected TOV21G cells when compared to the control (NT) (90.0 % ± 1.4 % vs 11.7 % ± 3.8 %, respectively; Fig 2 b). Further, compared to NT transfected cells, a high amount of miR-493-3p transfected TOV21G cells showed a low ΔΨm (10.6 % ± 1.3 % vs 59.9 % ± 3.9 %, respectively). In addition, also a large number of hsa-miR-493-3p transfected SKOV3 and OVCAR3 cells showed a low ΔΨm compared to the control (NT) (55.3 % ± 2.3 % vs 68.1 % ± 4.5 %, respectively; Fig 2 c). The DT control as well as the chemotherapeutic drug Paclitaxel led to the strongest loss of ΔΨm in these cell lines. At the level of fragmented DNA, high apoptosis induction was detected in hsa-miR-493-3p transfected SKOV3 and TOV21G cells (48.3 % ± 0.7 % vs. 17.2 % ± 0.3 % in NT transfected SKOV3 cells, 50.6 % ± 0.3 % vs. 17.8 % ± 1.4 % in NT transfected TOV21G cells; Fig 2 d).

To obtain more detailed data about the time course of apoptosis induced by miR-493-3p, long-term video-microscopy using the IncuCyte ZOOM Live-Cell Analysis System was applied. SKOV3 cells were analysed as they previously showed the highest induction of DNA fragmentation. Cells were grown for 72 h and stained with IncuCyte AnnexinV Red Reagent for apoptosis. The number of AnnexinV positive cells after treatment with miR-493-3p or Carboplatin steadily increased and reached a 1.8 and 2.2 fold higher level when compared to NT or Dimethyl sulfoxide (DMSO) treated cells, respectively. A significant increase of $p<0.05$ was analysed by two-way ANOVA

followed by Bonferroni post-test. It showed for Carboplatin treated cells after 49 h and for hsa-miR-493-3p transfected cells after 55 h significant differences compared to NT transfected cells (Fig 3 a).

A further hallmark of apoptosis is the activation of the effector caspases 3 and -7, that play important roles in the intrinsic as well as extrinsic apoptotic pathways [31]. Therefore, the analysis of caspase 3 and -7 activity was performed to examine the molecular changes induced after miR-493-3p transfection. The activation of caspase 3 and -7 was detected by long-term video-microscopy using the IncuCyte ZOOM Live-Cell Analysis System together with the IncuCyte Caspase-3/7 Green Apoptosis Assay Reagent. Caspase activity significantly ($p<0.05$; analysed by two-way ANOVA followed by Bonferroni post-test) increased 43 h after cell transfection with miR-493-3p, and 49 h after treatment with Carboplatin, while in NT and DMSO treated cells nearly no increase in caspase activity was detectable (Fig 3 b). In order to confirm the caspase activation by Western Blotting, protein lysates were prepared 72 h after treatment or transfection. 30 µM zVAD was used as caspase inhibitor [32]. After treating the cells with the chemotherapeutic drug Carboplatin, as well as after transfection with death control siRNA (DT) or hsa-miR-493, an induction of caspase 3 and PARP cleavage was observed. The amount of cleaved PARP was reduced in cells treated with zVAD and the pattern of cleaved caspase 3 was altered as the fragment of 12 kDa was undetectable (Fig 3 c).

Besides apoptosis induction cell motility after transfection was analysed by cell motility assay. 24 h after transfection, miR-493-3p transfected SKOV3 cells left a 1.5 broader gap than NT or untreated cells (miR-493-3p: 297 µm ± 131 µm, NT: 188 µm ± 70 µm, untreated: 114 µm ± 65 µm). Cells transfected with the death control siRNA (DT) hardly grew into the gap (Fig 3 d and e).

Altogether, these data strongly suggest a potential role of miR-493-3p in the regulation of cellular growth in different ovarian CA cells. However, only little is known about miR-493-3p regulated target genes which are involved in signalling pathways leading to the detected effects of apoptosis.

Gene and pathway regulation by miR-493-3p through direct binding partners

In order to investigate involved signalling pathways and critical downstream effectors leading to apoptosis after transient transfection of miR-493 in ovarian CA cells, we aimed to identify potential miR-493-3p target genes. First an *in silico* target gene prediction analysis for miR-493-3p using six different prediction databases was performed followed by a functional clustering analysis using Ingenuity Pathway Analysis (Qiagen Bioinformatics). Focusing on survival promoting or anti-apoptotic functions as well as ovarian CA signalling, the four target genes including Signal Transducer And Activator Of Transcription 3 (STAT3), High Mobility Group AT-Hook 2 (HMGA2), Mitogen-Activated Protein Kinase Kinase 5 (MAP2K5) and AKT Serine/Threonine Kinase 2 (AKT2) were selected for further analysis (Table 1, upper part). In addition, the data set for “Ovarian serous cystadenocarcinoma” from the cancer genome atlas (TCGA) data base served for negative correlation of miR-493 expression and potential target mRNAs as well as protein expression. In this study, a correlation with a p-value lower than 0.1 was considered as significant. The number of potential targets was reduced to twelve by *in silico* binding site prediction and clustering using PANTHER analysis [33] (Table 1, middle and lower part).

To analyse the potential regulation of those identified sixteen target genes (Table 1), SKOV3 and OVCAR3 cells were transiently transfected with miR-493-3p or NT and the mRNA expression analysed by qRT-PCR 48 h later. Four putative target genes were confirmed to be significantly downregulated in both cell lines after miR-493-3p

transfection (Fig 4 a), including Forkhead Box M1 (FOXM1), Fragile X Mental Retardation 1 (FMR1P), RAF1 Proto-Oncogene, Serine/Threonine Kinase (RAF1) and Serine/Threonine Kinase 38 Like (STK38L). Four additional putative targets were significantly downregulated in at least one cell line, including HMGA2, Mitogen-Activated Protein Kinase 1 (MAPK1), AKT2 and STAT3.

Focusing on these eight downregulated genes, we investigated the regulatory activity of miR-493-3p at protein expression level by Western Blotting. Protein lysates were prepared 60 h after transient transfection of miR-493-3p in SKOV3 and OVCAR3 cells. As shown in Fig 4 b, a major downregulation was observed for RAF1, AKT2 and HMGA2 in both cell lines followed by FOXM1, FMR1P and STK38L. No regulation on protein level was observed for MAPK1 and STAT3.

Next, we tested whether miR-493 directly modulated the downregulated genes via miRNA/mRNA interaction. Thus, AKT2, HMGA2, STK38L, FOXM1, RAF1 and FMR1P were assessed for direct interactions with hsa-miR-493-3p. Predicted binding sites in the 3' UTR of the mRNAs (Table 2 upper part, TargetScanHuman [34] and microRNA.org [35]) were cloned into the 3' UTR of a luciferase reporter gene of the pmirGLO Dual-Luciferase miRNA target expression vector and transfected together with miR-493-3p mimic, miRNA inhibitor anti-miR-493-3p or a non-targeting siRNA control into HEK293T cells as they represent an easy to transfect cell system for plasmids [36]. Luciferase activity was determined 72 h after transfection. The activity was significantly reduced with the binding site of AKT2 as well as with each of the two binding sites for HMGA2 and STK38L. The latter one revealed luciferase activity which was reduced to a minimum of 0.5 fold ± 0.04 fold for its second binding site. Anti-miR-493-3p had no or only a marginal effect on luciferase activity (Fig 4 c). To confirm the binding sites, mutations lacking the seed sequence of the predicted binding site (lacking red nucleotides in Table 2 upper part), were cloned into the 3'

UTR of a luciferase reporter gene and transfected into HEK293T cells together with miR-493-3p or NT. As shown in Fig 4 d the previously detected reduction in luciferase activity was abolished. Taken together, our data indicate that AKT2, HMGA2 and STK38L are direct targets of miR-493-3p leading to apoptosis in ovarian carcinoma cell lines, while RAF1, FOXM1 and FMR1P are regulated in an indirect manner.

Analysis of downstream signalling induced by direct targets of miR-493-3p leading to apoptosis

In order to examine underlying signalling pathways induced by miR-493-3p leading to apoptosis in more detail, we examined possible pro-apoptotic signal cascades downstream of the identified direct targets of miR-493-3p. As shown above, miR-493-3p transfected cells showed a decreased expression of AKT2. The analysis of myeloid cell leukaemia 1 (MCL1), a signalling molecule downstream of AKT2, showed a reduced expression together with a higher rate of cleavage when analysed by Western Blotting after transfection of miR-493-3p (Fig 5 a). It is known that MCL1 binds to Bak and Bax and therefore no longer inhibits the formation of pores in the mitochondrial membrane [37]. Western Blot analysis of these proteins showed that the expression of the pro-apoptotic Bak was induced, whereas the expression of the anti-apoptotic B-cell lymphoma-extra large (Bcl-XL) was reduced (Fig 5 a). These data may explain the observed release of cytochrome C (Fig 2 b), the reduction of mitochondrial potential (Fig 2 c) and the detected cleavage of caspase 3 together with the activation of PARP induced by transfection of miR-493-3p.

To further assess the significance of the identified direct binding partners of miR-493 in ovarian CA, TCGA data of ovarian serous cystadenocarcinoma patients were subsequently employed to analyse the survival time of high and low expressers of

mRNA/miR-493-3p binding partners. For AKT2 and STK38L, older patients (older than 67.5 years) showed a longer median survival. Patients expressing low levels of AKT2 lived 11.5 month longer than high expressers (Fig 5 b), whereas patients with a low expression of STK38L lived 7.4 month longer compared to high expressers (Fig 5 c).

Analysis of indirect regulation of RAF1 expression by miR-493-3p

The analysis of target gene regulation by miR-493-3p revealed a pronounced downregulation of RAF1 mRNA and protein levels (Fig 4 a and b). However, no direct binding of miR-493-3p to identified binding sites in RAF1 mRNA was observed (Fig 4 c and d). Since these data point towards an efficient but indirect regulation of RAF1 by miR-493-3p, it was of interest to identify underlying regulatory pathways. Therefore, a transcription analysis using the GeneChip Human Gene ST 2.0 Array was performed. Comparing RNA expression of miR-493-3p and NT transfected SKOV3 cells, 390 annotated genes were reduced in their expression after miR-493-3p transfection. Of these, 30 genes were coding for transcription factors, whereof twelve genes were predicted by microRNA.org [35] to have binding sites for miR-493-3p (Table 3). Out of these, ETS proto-oncogene 1 and 2 (ETS1 and ETS2), E2F transcription factor 5 (E2F5) and QKI, KH domain containing RNA binding (QKI) had previously been reported in connection with RAF1 [38] [39] [40] [41]. To verify potential regulation by miR-493-3p, qRT-PCR was carried out 48 h after miRNA transfection into SKOV3 cells and the highest downregulation was observed for ETS1 mRNA (0.1 fold ± 0.05 fold), followed by E2F5, ETS2 and QKI (0.5 fold ± 0.05 fold; Fig 6 a). To assess the downregulation on protein level, Western Blotting was performed with protein lysates 60 h after miR-493-3p transfection into SKOV3 cells. As shown in Fig 6 b, ETS1 and QKI protein expression was reduced, while ETS2 and

E2F5 protein expression was not influenced by miR-493-3p overexpression. In order to test whether miR-493 directly regulates ETS1, ETS2, QKI or E2F5 on transcript level, predicted binding sites in the 3' UTR of the mRNAs (Table 2 lower part, TargetScanHuman [34] and microRNA.org [35]) were cloned into the 3' UTR of a luciferase reporter gene of the pmirGLO Dual-Luciferase miRNA target expression vector. The vectors were transfected together with miR-493-3p mimic, miRNA inhibitor anti-miR-493-3p or a non-targeting siRNA control into HEK293T cells. The luciferase activity was significantly reduced for all three binding sites of ETS1 (ETS1_1 0.7 fold ± 0.04 fold, ETS1_2 0.7 fold ± 0.1 fold and for ETS1_3 0.8 fold ± 0.04 fold) as well as for the binding site of E2F5 with a fold change of 0.8 fold ± 0.03 fold. In contrast, QKI- and ETS2 binding sites as well as the anti-miR-493-3p had no influence on the reduction of luciferase activity (Fig 6 c). To confirm the binding sites, mutations lacking the seed sequence of the predicted binding site (lacking red nucleotides in Table 2 upper part), were cloned into the 3' UTR of a luciferase reporter gene. As shown in Fig 6 d the previously detected reduction in luciferase activity was abolished for ETS1 and E2F5.

Taken together, our data demonstrate that miR-493-3p directly regulated ETS1 and E2F5 mRNA expression. However, since E2F5 does not seem to be regulated on protein level, ETS1 is the most relevant transcription factor candidate for the observed regulation of RAF1 transcription.

To further investigate the possible regulation of RAF1 by ETS1, SKOV3 cells were transfected with siRNA against ETS1 or miR-493-3p. 48 h after transfection RNA was isolated and qRT-PCR performed against ETS1 and RAF1. As shown in Fig 6 e, transfection of siRNA against ETS1 led to a knockdown of the ETS1 mRNA and reduction of the RAF1 expression to 0.7 fold ± 0.08 fold. Western Blotting revealed a significant reduction of ETS1 protein expression after siRNA transfection. Further, the

expression of RAF1 was reduced both after transfection of the ETS1 siRNA or miR-493 (Fig 6 f). Taken together, our data indicate that miR-493-3p directly downregulates the transcription factor ETS1 leading to reduced transcription and expression of RAF1. To underscore the obtained data, we next analysed whether the ETS1 siRNA might phenocopy the observed induction of apoptosis by miR-493. Therefore, SKOV3 cells were transfected with ETS1 siRNA and the amount of apoptosis measured after 72 h by Nicoletti assay, demonstrating a reduction of apoptosis of 34.6 % ± 1.6 %, as measured by cells with fragmented DNA (Fig 6 g).

Regulation of RAF1 by interaction with STK38L

As described above, the expression of RAF1 mRNA and protein was clearly reduced after miR-493-3p transfection. One regulatory mechanism can be accomplished via the transcription factor ETS1, nonetheless, also protein:protein interaction followed by degradation can be an underlying regulation mechanism. An interaction of RAF1 and STK38L, (the latter one a direct binding partner of miR-493 as shown above), was predicted by PIPs: Human protein-protein interactions prediction [42]. To assess the possible interaction of both proteins, co-immunoprecipitations were performed to verify this prediction. RAF1 and STK38L were immunoprecipitated and blotted for both proteins as well as their interaction in untreated SKOV3 cells (Fig 7 a). Immunoprecipitation with anti-RAF1 followed by Western Blotting with anti-STK38L revealed a moderate interaction of both proteins which was increased when anti-STK38L precipitates were blotted with RAF1 antibodies (Fig 7 a). This latter observation might be due to the different affinities and avidities of both antibodies. Further, to test whether STK38L also phosphorylates RAF1, Flag tagged STK38L wild-type (Flag-STK38L WT) as well as a kinase dead version (Flag-STK38L KD) [43] were transfected into HEK293T cells. 48 h after transfection cells were

immunoprecipitated with anti-RAF1. Blotting with anti-Flag antibody showed comparable expression of STK38L (Fig 7b, right panel). Cell lysates blotted with anti-GAPDH revealed equal sample loading. However, blotting with anti-RAF1 or anti-phospho RAF1 serine 621 (Ser621) revealed that transfection with Flag-STK38L WT increased RAF1 expression and phosphorylation at Ser621 compared to untransfected cells (lane 2 vs lane 1) or Flag-STK38L KD transfectants (lane 2 vs lane 3) (Fig 7 b left panel). As shown in Fig 7 b, RAF1 phosphorylation at Ser621 is less in cells transfected with Flag-STK38L KD when compared to untransfected or Flag-STK38L WT overexpressing cells. These data point to a regulation of RAF1 protein level via interaction with STK38L which upon downregulation by miR-493-3p might lead to less phosphorylation at Ser621 and subsequent proteosomal degradation [44].

Discussion

Performing a high throughput screen of 188 miRNAs in four different cell lines we identified several novel pro-apoptotic miRNAs [18] including miR-493-3p. A potential downregulation of miR-493 in ovarian CA cell lines is supported by Wyman et al. describing a downregulation of hsa-miR-493 in stage III/IV epithelial ovarian CA compared to normal HOSE cells [45]. MiR-493 is also downregulated in other tumour types, for example in lung or gastric CA leading to apoptosis [21] [23]. However, the function and regulation of apoptosis by miR-493 in ovarian cancer cells still remains unknown. Hence, the pro-apoptotic effect of miR-493 was determined by flow cytometric measurements and potential targets of miR-493 were identified.

Transfection of miR-493 in the various ovarian carcinoma cell lines resulted in cell responses such as changes in the percentage of cell confluency and an increase in DNA laddering (cells in Sub G0/G1 phase). Long term measurements revealed a clear induction of apoptotic markers like AnnexinV and the activation of caspase 3. The observed apoptotic effects might be p53 independent due to the fact that the tumour suppressor p53 is mutated in these cell lines (SKOV3^{p53null}, OVCAR3^{p53R248Q} [27], TOV112D^{p53R175H} [28], A2780-cis^{p53K351N} [29] [30]). MiRNAs might offer the opportunity to overcome p53 dependent treatment resistance by triggering the cells with miRNA-493-3p.

Since miRNAs are known to have the potential to control a multiplicity of target genes [46], the aim of this study was to identify the network of target genes that is regulated by miR-493-3p and causative for the observed pro-apoptotic functions. *In silico* target prediction in several databases (as described above) were used to find potential mRNA targets with a binding site for direct interaction with miR-493.

In this study, we demonstrate that miR-493 overexpression resulted in diminished FOXM1 and AKT2 protein expression (Fig 4 b). AKT2 was found to be a potential

direct target of miR-493 by luciferase assay. Activation of the MAPK/ERK pathway leads to cell survival and proliferation by stimulating transcription factors such as proto-oncogene c-myc or Ets like protein 1 (Elk1) [2]. Downregulation of proteins involved in both, the MAPK/ERK as well as the PI3-kinase – AKT pathway leads to activation of the transcription factor FOXO3 [47]. Phosphorylation of FOXO3 causes its inhibition and translocation from the nucleus into the cytoplasm. FOXO3 is involved in the regulation of metabolism, apoptosis and DNA repair [48]. Reduction of AKT2 together with the activation of FOXO3 results in diminished FOXM1 activity. FOXM1 activates the transcription of mRNAs needed for cell cycle regulation or DNA repair [48] (Fig 7 c). MiR-493 was shown to bind directly to the 3' UTR of AKT2 (Fig 4 c and d). AKT2, the key downstream effector of the PI3-kinase pathway, is best known for its anti-apoptotic effects [49]. Downregulation of AKT2 in non-small cell lung cancer (NSCLC) leads to cleavage of the induced myeloid leukaemia cell differentiation protein MCL1. MCL1 belongs to the Bcl-2 family and by binding to Bak and Bax it inhibits the formation of pores in the mitochondrial membrane [37]. Hence, a decrease of MCL1 mediated by decreased AKT2 levels resulted in a loss of mitochondrial potential and release of cytochrome C [50]. Further, the release of cytochrome C (Fig 2 b) and the alteration of mitochondrial membrane permeability modulate proteins of the Bcl2 family like Bak leading to apoptosis via the activation of effector caspases (Fig 7 c) [1].

Kaplan-Meier Blots with ovarian serous cystadenocarcinoma patients (data from TCGA) suggested that patients with lower AKT2 expression had a longer median survival (Fig 5 b). In line with that, Zhu et al. observed in osteosarcoma patients that a low expression level of AKT2 correlates with a better prognosis [51].

With the reduced expression of AKT2 after miR-493 transfection the amount of FMR1P protein was reduced (Fig 4 b). Mechanistic Target of Rapamycin (mTOR), a

major regulator of protein synthesis, is activated by AKT mediated phosphorylation. Activated mTOR phosphorylates downstream ribosomal protein S6 kinase beta-1 (S6K1) at threonine 389 leading to the activation of FMR1P [52]. FMR1P acts as a shuttle by transporting mRNA from the nucleus to the cytoplasm. Diminished expression of FMR1P is described to lead to mental retardation [53].

Another target directly regulated by miR-493-3p is High Mobility Group AT-Hook 2 (HMGA2). HMGA2 co-localizes with key replication factors and therefore stabilizes branched DNA structures *in vitro.* Yu et al. demonstrated that HMGA2 prevents double strand brakes at stalled replication forks and enhances cell survival [54]. Consequently, reduced HMGA2 levels, induced by miR-493-3p, led to apoptosis and DNA fragmentation as described in this study (Fig 7 c). However, the underlying mechanisms of HMGA2 mediated apoptosis are still unknown. Strikingly, although there was obviously no interaction of miR-493 and RAF1 binding site, a significant downregulation on mRNA and protein level was detected. ETS1 a direct target of miR-493-3p, was identified as a potential transcription factor for RAF1. Silencing ETS1 significantly reduces the transcription of RAF1. Although the effects of ETS1 on apoptosis are reported to be controversial [55], in our system knockdown of ETS1 clearly revealed pro-apoptotic effects (Fig 6 g). Furthermore, ETS1 might also regulate RAF1 expression via the regulation of VEGF [55] that is modulating the MAPK/ERK pathway (Fig 7 d).

STK38L also known as Nuclear Dbf2-related (NDR) protein kinase (NDR2) was identified as another direct miR-493-3p binding partner showing reduced protein levels after miR-493 transfection. Furthermore, the predicted interaction (PIPs: Human protein-protein interactions prediction [42]) between the serine/threonine kinase STK38L and RAF1 was experimentally confirmed. It is reported that knockdown of STK38L results in cell cycle arrest and reduction of cell proliferation as

well as upregulation of apoptosis [56] [57]. Notably, we observed that STK38L phosphorylates RAF1 at Ser621. Autophosphorylation at Ser621 is a key step in stabilizing the kinase by binding to 14-3-3 proteins and prevention of proteasomal degradation [44]. STK38L mediated RAF1 phosphorylation at this site might augment these effects since a kinase dead form of STK38L reduced RAF1 phosphorylation at Ser621 resulting in reduced RAF1 protein level. Due to the fact that miR-493-3p diminished the expression of STK38L, RAF1 phosphorylation at Ser621 is diminished, making the kinase potentially more prone for degradation (Fig 7 d) [44].

E2F5 was found to be another transcription factor modulated by miR-493. E2F5 binds to the promoters of target genes involved in cell cycle control thereby regulating cell growth and proliferation [58]. Downregulation of E2F5 via miR-493 or other miRNAs is reported to influence apoptosis as well as cell proliferation, invasion and cell motility in ovarian cancer cells [58].

In summary, miR-493-3p was validated to induce apoptosis in different ovarian CA cell lines. AKT2, HMGA2, ETS1, E2F5 and STK38L were identified as novel players, contributing to our understanding of the molecular mechanisms of network regulation by miR-493-3p mediated apoptosis. ETS1 as well as STK38L were found as potentially new regulators for transcription and phosphorylation of RAF1, respectively. Our findings that miR-493 regulates certain signalling pathways leading to apoptosis may have clinical relevance in regards to the development of new therapy strategies for ovarian cancer patients.

Methods

Cell culture

T98G (CRL-1690, LGC Standards, Wesel, Germany), HCT116 (CCL-247, LGC Standards), OVCAR3, TOV21G and TOV112D [28] were cultured in RPMI-1640 medium (Th Geyer, Renningen, Germany). HOSE 2170 [26], SGBS [59], HEK293T (CRL-3216, LGC Standards) and SKOV3 (HTB-77, LGC Standards) cells were cultured in DMEM high glucose medium (Th Geyer). The media contained 4 mM stable glutamine and were supplemented with 10% (v/v) FBS (Sigma-Aldrich, München, Germany). A2780 and A2780-cis cells were grown in RPMI-1640 media with 20% (v/v) FBS. All cells were grown at 37 °C and 5% CO_2. The phenotype as well as the cell density of the adherent cell culture was proofed with the automated single well microscope NyOne (SynenTec Bio Services, Münster, Germany).

SKOV3 cells are p53 null and were also used in the previous cellular high throughput screening [18], therefore the assays were focused on this cell line. Additionally, the high invasive OVCAR3^{p53R248Q} cells [27] were used. Furthermore, the cell lines TOV21G, without p53 mutation, or TOV112D^{p53R175H} with p53 mutation [28] as well as A2780-cis^{p53K351N} with Cisplatin resistance or A2780 [29] [30] without Cisplatin resistance were included for apoptosis assays. HEK293T cells were used for luciferase assays and immunoprecipitations as they are an easy to transfect cell system for plasmids [36].

Transfection with miRNA mimics

The cells were seeded and transfected with 62.5 nM miRNA mimic (Qiagen, Hilden, Germany), non-targeting siRNA (AllStars Neg. control, order number: 1027281, negative control for cell death; NT), human cell death control siRNA (AllStars Cell Death control, order number: 1027299, positive control for cell death; DT; Qiagen) or

siRNA against ETS1 (siRNA ID: VH S40614, Thermo Fisher Scientific, Darmstadt, Germany). The miRNA or siRNA were transfected with ScreenFect A reagent (ScreenFect, Eggenstein-Leopoldshafen, Germany) as described before [60] [61]. As controls, the cells were treated with 25 µM Etoposide, 80 µM Carboplatin or 0.25 µM Paclitaxel (all reagents from Enzo Life Sciences, Lörrach, Germany). The transfection efficiency was surveyed by a fluorescent-labelled non-targeting siRNA. After transfection about 95 – 100% cells showed red fluorescence.

Analysis of apoptotic cells, detection of mitochondria potential and cytochrome C release

Apoptotic cells were identified by flow cytometry measuring the amount of cells with reduced DNA content (sub G0/G1) as previously described by Rudner et al. [62]. For detection of the mitochondrial potential of the cells, a TMRE assay was carried out as described by Flum et al [61]. To stain for free cytochrome C after mitochondrial damage, the cells were detached, fixed with 4% (w/v) paraformaldehyde for 15 min, permeabilised with 0.1% (v/v) Triton X-100 and stained with an Alexa Fluor 488 labelled antibody (BLD-612308; Biozol, Eching, Germany) against cytochrome C for 1 h in the dark. The antibody was diluted 1:1,500 in 5% BSA /TBST solution.The quantitative analysis was performed with the MACSQuant Analyser using fluorescence channel B1 (525/50 nm filter).

Cell motility Assay

For the analysis of cell motility 40,000 cells/ml were seeded into 96 well plates 24 h before transfection. Immediately before transfection a scratch was performed using 1000 µl pipet tips on a multi-channel pipette. To remove scratched cells, the wells were washed with PBS three times, after the transfection mix was added.

564 Immediately after transfection the cells were analysed with the automated single well
565 microscope NyOne.
566
567 **RT-PCR**
568 The extraction of total RNA was done using the miRNeasy Mini Kit (Qiagen, Hilden,
569 Germany). 1000 ng of isolated RNA was transcribed via the miScript II RT Kit
570 (Qiagen) using 5x miScript HiSpec Buffer and an incubation time of 60 min at 37 °C.
571 The 1:30 diluted cDNA was further analysed in the Roche Light Cycler 480 using
572 GreenMasterMix (Genaxxon Bioscience, Ulm, Germany). For the qRT-PCR reaction
573 the primers for hsa-miR-493-3p (5´- TGAAGGTCTACTGTGTGCCAGG-3`) or hsa-
574 miR-493-5p (5´- TTGTACATGGTAGGCTTTCATT-3`) were used together with the
575 universal reverse primer from the miScript PCR Starter Kit (Qiagen). U6 snRNA
576 primer forward (5´-CTCGCTTCGGCAGCACA-3´) and U6 snRNA primer reverse (5´-
577 AACGCTTCACGAATTTGCGT-3´) served for control loading. To analyse the
578 expression of potential target genes, 1000 ng of isolated RNA were transcribed using
579 the Transcriptor High Fidelity cDNA Synthesis Kit from Roche (Penzberg, Germany).
580 For detection of mRNA expression of potential targets the following primers were
581 used: ADAR1_FW (5´-CTGGATTCCACAGGGATTGT-3´), ADAR1_RV (5´-
582 TTCGAGAATCCCAAACAAGG-3´), AKT2_FW (5´-TGGGTCTGGAAGGCATACTT-
583 3´), AKT2_RV (5´-CTCACACAGTCACCGAGAGC-3´), ALKBH3_FW (5´-
584 TCCCATGATCCAAGGGTATC-3´), ALKBH3_RV (5´-
585 CACGCACATTTGAGATGAGAA-3´), E2F5_FW (5´-CGGCGTTCTGGATCTCAA-3´),
586 E2F5_RV (5´-CAATTCCCTCTAAGACATTGGTG-3´), EEF2K_FW (5´-
587 GCGCGAGCTTTTGACTCT-3´), EEF2K_RV (5´-AGGGCCTCTAGCCAGTCTTG-3´),
588 ETS1_FW (5´-CCATCATCAAGACGGAAAAAG-3´), ETS1_RV (5´-
589 GGGACATCTGCACATTCCATA-3´), ETS2_FW (5´-CAGCGTCACCTACTGCTCTG-

3′), ETS2_RV (5′-AGTCGTGGTCTTTGGGAGTC-3′), FMR1P_FW (5′-AATCCAAAAGAACAGTGGCATT-3′), FMR1P_RV (5′-GGAATCCCAGAAACCTGAACT-3′), FOXM1_FW (5′-CCACTGGATGTTGGATAGGC-3′), FOXM1_RV (5′-AGAAACGGGAGACCTGTGC-3′), GAB2_FW (5′-AGGGGCAGGACTGTTCGT-3′), GAB2_RV (5′-CGAAGAGAACTATGTCCCTATGC-3′), HMGA2_FW (5′-TCCCTCTAAAGCAGCTCAAAA-3′), HMGA2_RV (5′-ACTTGTTGTGGCCATTTCCT-3′), JAK2_FW (5′-CAGGAACAAGATGTGAACTGTTTC-3′), JAK2_RV (5′-CCCATGCAGAGTCTTTTTCAG-3′), MAP2K5_FW (5′-TCAGGGGAGCAGTATGGAAT-3′), MAP2K5_RV (5′-AAACCTCCCAAGAGCAAGC-3′), MAPK1_FW (5′-TCTGCACCGTGACCTCAA-3′), MAPK1_RV (5′-GCCAGGCCAAAGTCACAG-3′), PEA15_FW (5′-GTCCCGTACTCAGCCATGA-3′), PEA15_RV (5′-TTAGGAACCGGGGACTCA-3′), PIK3R3_FW (5′-GGCTTAGGTGGCTTTGGTG-3′), PIK3R3_RV(5′-TGATGCCCTATTCGACAGAA-3′), PPIA_FW (5′-ATGCTGGACCCAACACAAAT-3′), PPIA_RV (5′-TCTTTCACTTTGCCAAACACC-3′), QKI_FW (5′-CCAACTTCTGCGGGATCTT-3′), QKI_RV (5′-TGTCATTGTACATGTCTTTCCGTA-3′), RAF1_FW (5′-TGGGAAATAGAAGCCAGTGAA-3′), RAF1_RV (5′-CCTTTAGGATCTTTACTGCAACATC-3′), STAT3_FW (5′-CCCTTGGATTGAGAGTCAAGA-3′), STAT3_RV (5′-AAGCGGCTATACTGCTGGTC-3′), STK38L_FW (5′-CAAAGACCACCAGTCACACAA-3′) and STK38L_RV (5′-GAAGAAGAACAGGAGACAACTGG-3′).

Western Blotting

Protein analysis was conducted by Western Blotting as previously described [61]. The antibodies against Caspase-3 (cs#9662), cleaved Caspase-3 (cs#9664), PARP (cs#9542) and cleaved PARP (cs#9541) were from Cell Signaling Technology (Danvers, United States) and diluted 1:1,000. For analysis of molecular mechanisms, cells were treated with 30 µM zVAD (Enzo Life Sciences). For detection of target proteins the following antibodies were used: ETS1 (1:500; sc-55581), QKI (1:500; sc-517305), E2F5 (1:500; sc-374268) from Santa Cruz Biotechnology (Heidelberg, Germany), Bak (1:1000; cs#12105T), Bcl-XL (1:1000; cs#2764T), MCL1 (1:1000; cs#94296), RAF1 (1:1000; cs#53745), FMR1P (1:1000; cs#7104), FOXM1 (1:1000; cs#5436), HMGA2 (1:1000; cs#5269), MAPK1 (1:1000; cs#9102S) and STAT3 (1:1000; cs#9139) from Cell Signaling Technology as well as ETS1 (1:1000; orb393050; Biozol; Echingen, Germany), ETS2 (1:1000; CSB-PA007853LA01HU; Biozol), AKT2 (1:500; 680202; BioLegend, Fell, Germany), and STK38L (1:500; ABIN3185788; antikoerper-online.de, Aachen, Germany). The antibody against Flag (1:1000; F3156; Sigma Aldrich) was used to detect the Flag-tagged STK38L proteins. Depending on the size of the other proteins the antibodies against β-Actin (1:10,000; A5441; Sigma Aldrich) or GAPDH (1:5000; MA5-15738; Thermo Fisher Scientific) served as loading control.

The secondary antibody, anti-rabbit IgG, HRP-linked (cs#7074, Cell Signaling Technology) or anti-mouse IgG, HRP linked (A4416, Sigma Aldrich) was diluted 1:10,000.

Apoptosis assay with long-term video-microscopy

The activation of caspases was measured by long-term video-microscopy. The cells were transfected or treated with chemotherapeutic drugs as described above. 1 h after treatment, IncuCyte Caspase-3/7 Green Apoptosis Assay Reagent (Sartorius,

641 Goettingen, Germany) was added to a final concentration of 5 nM as well as
642 IncuCyte™ AnnexinV Red reagent with a final dilution of 1:200. The cells were
643 placed into the IncuCyte ZOOM Live-Cell Analysis System detecting red and green
644 fluorescence. The imaging system is placed in an incubator with standard culture
645 conditions. Images from each well at two different positions were taken automatically
646 every hour with a 20x objective and analysed with the IncuCyte ZOOM Software for
647 the amount of fluorescent stained cells. The data were visualized using GraphPad
648 Prism 5 software.
649
650 **TCGA-Analysis correlation**
651 To examine the correlation between the miR-493 expression and potential targets,
652 level 3 miRNA expression data of the “Ovarian serous cystadenocarcinoma” data set
653 were downloaded from the cancer genome atlas (TCGA) data base (www.tcga-
654 data.nci.nih.gov/tcga) using the “firehose-get“ command-line tool
655 (https://confluence.broadinstitute.org/display/GDAC/Download). A detailed
656 description of the clinical characteristics of the cohort can be found in a study by
657 Cancer Genome Atlas Research Network [63]. Additionally, the mRNA as well as the
658 protein expression of all these patients were downloaded and negatively correlated to
659 the miRNA expression of each of the 530 patients.
660 For the delineation of the survival of ovarian serous cystadenocarcinoma patients
661 affected by miR-493 binding partners (AKT2 and STK38L), different age groups
662 (range: 26–89 years, mean: 67.5 years) were analysed dividing the patients’ age in
663 first quartile, mean, median or third quartile. For each age group differential survival
664 analysis for patients with high- versus low-expression of AKT2 and STK38L was
665 conducted employing the median expression as threshold. For this, the log-rank test

was applied on the resulting cox-proportional hazard-models and for the purpose of visualization Kaplan-Meier Blots were generated.

Gene expression analysis

To analyse the differential gene expression after transfection the GeneChip Human Gene ST 2.0 Array (Thermo Fisher Scientific) was used. Reverse Transcription and biotin labelling of the RNA was carried out with the GeneChip WT PLUS Reagent Kit (Thermo Fisher Scientific). Hybridization and data analysis were performed as described previously [64].

***In silico* target prediction**

For identification of potential miR-493-3p target genes the prediction tools TargetScanHuman [34], microRNA.org [35], Rna22 [65], DIANA TOOLS [66], miRDB [67] and miRWalk [68] were used. The online gene classification software Protein Analysis Through Evolutionary Relationships (PANTHER) [69] was used to cluster the potential targets for apoptotic functions. Ingenuity Pathway Analysis (IPA, Qiagen Bioinformatics) was employed to suggest potential target genes restricted to genes with anti-apoptotic or survival promoting functions in ovarian CA signalling. Already experimentally validated miR-493-3p target genes listed in miRTarBase [70] and miRWalk [68] were excluded from further investigations.

Potential miR-493-3p binding sites were obtained from the database microRNA.org [35] as well as from TargetScanHuman [34].

Luciferase reporter assay

690 Luciferase reporter constructs were generated with oligonucleotide cloning.
691 Luciferase reporter assays were performed in HEK293T cells as described by Flum
692 et al. [61].
693
694 **Immunoprecipitation and immunoblotting**
695 40,000 HEK293T cells were seeded into 6-well culture pates. 24 h later, the cells
696 were transfected with 5 μg of STK38L WT (Addgene, Cambridge, USA) or 10 μg of
697 STK38L KD plasmid [43]. 48 h after transfection, cells were lysed in ice-cold lysis
698 buffer (1% Triton X-100, 20mM Tris, 150mM NaCl, pH 8.0) containing a cocktail of
699 protein inhibitors (Merck, Darmstadt, Germany). Post-nuclear lysates were incubated
700 for 1h with the indicated antibody. 30 μl of Protein A Sepaharose beads (Sigma
701 Aldrich, Darmstadt, Germany) were added and incubated for 1h at 4 °C.
702 Immunoprecipitates were washed four times with ice-cold lysis buffer and proteins
703 were eluted by boiling for 5 min in SDS sample buffer, separated by SDS-PAGE and
704 transferred onto PVDF membrane for immunoblotting. Membranes were blocked with
705 5% BSA in TBST (TBS, 1% Tween) and incubated with the indicated antibody for 1 h.
706 Bound antibody was revealed with the appropriate secondary antibody and protein
707 was visualized by chemiluminescence using Immobilon Western Chemiluminescent
708 HRP substrate (Thermo Fisher Scientific).
709
710 **Statistical analysis**
711 Data in general were expressed as mean ± SD. Statistical analysis was carried out
712 using GraphPad Prism Version 5.04. The corresponding statistical test and the level
713 of significance are indicated in each figure legend. For TCGA analysis all calculations
714 were conducted employing the R statistical platform [71] using functions from the
715 CRAN package survival (www.cran.r-project.org/web/packages/survival).

716

717

Ethical standards

The authors declare that the experiments comply with the current laws of the Federal Republic of Germany.

Conflict of interest

The authors declare that they have no conflict of interest.

References

1 Elmore S (2007) Apoptosis: a review of programmed cell death. Toxicol Pathol 35 (4):495-516. doi:10.1080/01926230701320337

2 Zhang W, Liu HT (2002) MAPK signal pathways in the regulation of cell proliferation in mammalian cells. Cell Res 12 (1):9-18

3 Cory S, Adams JM (2002) The Bcl2 family: regulators of the cellular life-or-death switch. Nature reviews Cancer 2 (9):647-656. doi:10.1038/nrc883

4 Chaitanya GV, Alexander JS, Babu PP (2010) PARP-1 cleavage fragments: signatures of cell-death proteases in neurodegeneration. Cell Communication and Signaling : CCS 8:31-31. doi:10.1186/1478-811X-8-31

5 Kaufmann SH, Mesner PW, Jr., Samejima K, Tone S, Earnshaw WC (2000) Detection of DNA cleavage in apoptotic cells. Methods in enzymology 322:3-15

6 He L, Hannon GJ (2004) MicroRNAs: small RNAs with a big role in gene regulation. Nat Rev Genet 5 (7):522-531

7 MacFarlane L-A, Murphy PR (2010) MicroRNA: Biogenesis, Function and Role in Cancer. Current Genomics 11 (7):537-561. doi:10.2174/138920210793175895

8 Kim VN, Han J, Siomi MC (2009) Biogenesis of small RNAs in animals. Nat Rev Mol Cell Biol 10 (2):126-139. doi:10.1038/nrm2632

9 Filipowicz W, Bhattacharyya SN, Sonenberg N (2008) Mechanisms of post-transcriptional regulation by microRNAs: are the answers in sight? Nat Rev Genet 9 (2):102-114. doi:10.1038/nrg2290

10 Lynam-Lennon N, Maher SG, Reynolds JV (2009) The roles of microRNA in cancer and apoptosis. Biol Rev Camb Philos Soc 84 (1):55-71. doi:10.1111/j.1469-185X.2008.00061.x

11 Lima RT, Busacca S, Almeida GM, Gaudino G, Fennell DA, Vasconcelos MH (2011) MicroRNA regulation of core apoptosis pathways in cancer. Eur J Cancer 47 (2):163-174. doi:10.1016/j.ejca.2010.11.005

12 Adams JM, Cory S (2007) The Bcl-2 apoptotic switch in cancer development and therapy. Oncogene 26 (9):1324-1337. doi:10.1038/sj.onc.1210220

13 Pal MK, Jaiswar SP, Dwivedi VN, Tripathi AK, Dwivedi A, Sankhwar P (2015) MicroRNA: a new and promising potential biomarker for diagnosis and prognosis of ovarian cancer. Cancer Biol Med 12 (4):328-341. doi:10.7497/j.issn.2095-3941.2015.0024

14 Siegel RL, Miller KD, Jemal A (2017) Cancer Statistics, 2017. CA Cancer J Clin 67 (1):7-30. doi:10.3322/caac.21387

15 Karst AM, Drapkin R (2010) Ovarian cancer pathogenesis: a model in evolution. J Oncol 2010:932371. doi:10.1155/2010/932371

16 Della Pepa C, Tonini G, Pisano C, Di Napoli M, Cecere SC, Tambaro R, Facchini G, Pignata S (2015) Ovarian cancer standard of care: are there real alternatives? Chin J Cancer 34 (1):17-27. doi:10.5732/cjc.014.10274

17 Chang L, Graham P, Hao J, Ni J, Deng J, Bucci J, Malouf D, Gillatt D, Li Y (2016) Cancer stem cells and signaling pathways in radioresistance. Oncotarget 7 (10):11002-11017. doi:10.18632/oncotarget.6760

18 Kleemann M, Bereuther J, Fischer S, Marquart K, Hanle S, Unger K, Jendrossek V, Riedel CU, Handrick R, Otte K (2016) Investigation on tissue specific effects of pro-apoptotic micro RNAs revealed miR-147b as a potential biomarker in ovarian cancer prognosis. Oncotarget. doi:10.18632/oncotarget.13095

19 Lima RT, Busacca S, Almeida GM, Gaudino G, Fennell DA, Vasconcelos MH (2011) MicroRNA regulation of core apoptosis pathways in cancer. European Journal of Cancer 47 (2):163-174. doi:https://doi.org/10.1016/j.ejca.2010.11.005

20 Li J, Liang S, Jin H, Xu C, Ma D, Lu X (2012) Tiam1, negatively regulated by miR-22, miR-183 and miR-31, is involved in migration, invasion and viability of ovarian cancer cells. Oncology reports 27 (6):1835-1842. doi:10.3892/or.2012.1744

21 Gu Y, Cheng Y, Song Y, Zhang Z, Deng M, Wang C, Zheng G, He Z (2014) MicroRNA-493 Suppresses Tumor Growth, Invasion and Metastasis of Lung Cancer by Regulating E2F1. PLoS ONE 9 (8):e102602. doi:10.1371/journal.pone.0102602

782 22 Ueno K, Hirata H, Majid S, Yamamura S, Shahryari V, Tabatabai ZL, Hinoda Y,
783 Dahiya R (2012) Tumor suppressor microRNA-493 decreases cell motility and migration
784 ability in human bladder cancer cells by down-regulating RhoC and FZD4. Molecular cancer
785 therapeutics 11 (1):244-253. doi:10.1158/1535-7163.MCT-11-0592
786 23 Zhou W, Zhang C, Jiang H, Zhang Z, Xie L, He X (2015) MiR-493 suppresses the
787 proliferation and invasion of gastric cancer cells by targeting RhoC. Iranian Journal of Basic
788 Medical Sciences 18 (10):1027-1033
789 24 Benetatos L, Hatzimichael E, Londin E, Vartholomatos G, Loher P, Rigoutsos I,
790 Briasoulis E (2013) The microRNAs within the DLK1-DIO3 genomic region: involvement in
791 disease pathogenesis. Cellular and molecular life sciences : CMLS 70 (5):795-814.
792 doi:10.1007/s00018-012-1080-8
793 25 Benetatos L, Vartholomatos G, Hatzimichael E (2014) DLK1-DIO3 imprinted cluster in
794 induced pluripotency: landscape in the mist. Cellular and molecular life sciences : CMLS 71
795 (22):4421-4430. doi:10.1007/s00018-014-1698-9
796 26 Choi P-W, Yang J, Ng S-K, Feltmate C, Muto MG, Hasselblatt K, Lafferty-Whyte K,
797 JeBailey L, MacConaill L, Welch WR, Fong W-P, Berkowitz RS, Ng S-W (2016) Loss of E-
798 cadherin disrupts ovarian epithelial inclusion cyst formation and collective cell movement in
799 ovarian cancer cells. Oncotarget 7 (4):4110-4121. doi:10.18632/oncotarget.6588
800 27 Kobayashi M, Salomon C, Tapia J, Illanes SE, Mitchell MD, Rice GE (2014) Ovarian
801 cancer cell invasiveness is associated with discordant exosomal sequestration of Let-7
802 miRNA and miR-200. J Transl Med 12:4. doi:10.1186/1479-5876-12-4
803 28 Samouelian V, Maugard CM, Jolicoeur M, Bertrand R, Arcand SL, Tonin PN,
804 Provencher DM, Mes-Masson AM (2004) Chemosensitivity and radiosensitivity profiles of
805 four new human epithelial ovarian cancer cell lines exhibiting genetic alterations in BRCA2,
806 TGFbeta-RII, KRAS2, TP53 and/or CDNK2A. Cancer chemotherapy and pharmacology 54
807 (6):497-504. doi:10.1007/s00280-004-0843-9
808 29 Behrens BC, Hamilton TC, Masuda H, Grotzinger KR, Whang-Peng J, Louie KG,
809 Knutsen T, McKoy WM, Young RC, Ozols RF (1987) Characterization of a cis-

diamminedichloroplatinum(II)-resistant human ovarian cancer cell line and its use in evaluation of platinum analogues. Cancer Res 47 (2):414-418

30 Masuda H, Ozols RF, Lai GM, Fojo A, Rothenberg M, Hamilton TC (1988) Increased DNA repair as a mechanism of acquired resistance to cis-diamminedichloroplatinum (II) in human ovarian cancer cell lines. Cancer Res 48 (20):5713-5716

31 Strasser A, O'Connor L, Dixit VM (2000) Apoptosis signaling. Annu Rev Biochem 69:217-245. doi:10.1146/annurev.biochem.69.1.217

32 Garcia-Calvo M, Peterson EP, Leiting B, Ruel R, Nicholson DW, Thornberry NA (1998) Inhibition of human caspases by peptide-based and macromolecular inhibitors. J Biol Chem 273 (49):32608-32613

33 Mi H, Muruganujan A, Thomas PD (2013) PANTHER in 2013: modeling the evolution of gene function, and other gene attributes, in the context of phylogenetic trees. Nucleic acids research 41 (Database issue):D377-386. doi:10.1093/nar/gks1118

34 Agarwal V, Bell GW, Nam JW, Bartel DP (2015) Predicting effective microRNA target sites in mammalian mRNAs. eLife 4. doi:10.7554/eLife.05005

35 Betel D, Koppal A, Agius P, Sander C, Leslie C (2010) Comprehensive modeling of microRNA targets predicts functional non-conserved and non-canonical sites. Genome Biology 11 (8):R90. doi:10.1186/gb-2010-11-8-r90

36 Fischer S, Buck T, Wagner A, Ehrhart C, Giancaterino J, Mang S, Schad M, Mathias S, Aschrafi A, Handrick R, Otte K (2014) A functional high-content miRNA screen identifies miR-30 family to boost recombinant protein production in CHO cells. Biotechnol J 9 (10):1279-1292. doi:10.1002/biot.201400306

37 Thomas LW, Lam C, Edwards SW (2010) Mcl-1; the molecular regulation of protein function. FEBS Lett 584 (14):2981-2989. doi:10.1016/j.febslet.2010.05.061

38 Lassmann S, Weis R, Makowiec F, Roth J, Danciu M, Hopt U, Werner M (2007) Array CGH identifies distinct DNA copy number profiles of oncogenes and tumor suppressor genes in chromosomal- and microsatellite-unstable sporadic colorectal carcinomas. Journal of molecular medicine (Berlin, Germany) 85 (3):293-304. doi:10.1007/s00109-006-0126-5

838 39 Zhang SX, Garcia-Gras E, Wycuff DR, Marriot SJ, Kadeer N, Yu W, Olson EN, Garry
839 DJ, Parmacek MS, Schwartz RJ (2005) Identification of direct serum-response factor gene
840 targets during Me2SO-induced P19 cardiac cell differentiation. The Journal of biological
841 chemistry 280 (19):19115-19126. doi:10.1074/jbc.M413793200
842 40 Iorns E, Turner NC, Elliott R, Syed N, Garrone O, Gasco M, Tutt AN, Crook T, Lord
843 CJ, Ashworth A (2008) Identification of CDK10 as an important determinant of resistance to
844 endocrine therapy for breast cancer. Cancer cell 13 (2):91-104.
845 doi:10.1016/j.ccr.2008.01.001
846 41 Jain P, Fierst TM, Han HJ, Smith TE, Vakil A, Storm PB, Resnick AC, Waanders AJ
847 (2017) CRAF gene fusions in pediatric low-grade gliomas define a distinct drug response
848 based on dimerization profiles. Oncogene 36 (45):6348-6358. doi:10.1038/onc.2017.276
849 42 McDowall MD, Scott MS, Barton GJ (2009) PIPs: human protein-protein interaction
850 prediction database. Nucleic Acids Res 37 (Database issue):D651-656.
851 doi:10.1093/nar/gkn870
852 43 Devroe E, Erdjument-Bromage H, Tempst P, Silver PA (2004) Human Mob proteins
853 regulate the NDR1 and NDR2 serine-threonine kinases. The Journal of biological chemistry
854 279 (23):24444-24451. doi:10.1074/jbc.M401999200
855 44 Noble C, Mercer K, Hussain J, Carragher L, Giblett S, Hayward R, Patterson C,
856 Marais R, Pritchard CA (2008) CRAF Autophosphorylation of Serine 621 Is Required to
857 Prevent Its Proteasome-Mediated Degradation. Molecular cell 31 (6):862-872.
858 doi:10.1016/j.molcel.2008.08.026
859 45 Wyman SK, Parkin RK, Mitchell PS, Fritz BR, O'Briant K, Godwin AK, Urban N,
860 Drescher CW, Knudsen BS, Tewari M (2009) Repertoire of microRNAs in Epithelial Ovarian
861 Cancer as Determined by Next Generation Sequencing of Small RNA cDNA Libraries. PLOS
862 ONE 4 (4):e5311. doi:10.1371/journal.pone.0005311
863 46 Fischer S, Handrick R, Aschrafi A, Otte K (2015) Unveiling the principle of microRNA-
864 mediated redundancy in cellular pathway regulation. RNA Biol 12 (3):238-247.
865 doi:10.1080/15476286.2015.1017238

47 Roy SK, Srivastava RK, Shankar S (2010) Inhibition of PI3K/AKT and MAPK/ERK pathways causes activation of FOXO transcription factor, leading to cell cycle arrest and apoptosis in pancreatic cancer. Journal of Molecular Signaling 5:10-10. doi:10.1186/1750-2187-5-10

48 Gomes AR, Zhao F, Lam EWF (2013) Role and regulation of the forkhead transcription factors FOXO3a and FOXM1 in carcinogenesis and drug resistance. Chinese Journal of Cancer 32 (7):365-370. doi:10.5732/cjc.012.10277

49 Zhang D, Piao HL, Li YH, Qiu Q, Li DJ, Du MR, Tsang BK (2016) Inhibition of AKT sensitizes chemoresistant ovarian cancer cells to cisplatin by abrogating S and G2/M arrest. Experimental and molecular pathology 100 (3):506-513. doi:10.1016/j.yexmp.2016.05.003

50 Lee MW, Kim DS, Lee JH, Lee BS, Lee SH, Jung HL, Sung KW, Kim HT, Yoo KH, Koo HH (2011) Roles of AKT1 and AKT2 in non-small cell lung cancer cell survival, growth, and migration. Cancer Sci 102 (10):1822-1828. doi:10.1111/j.1349-7006.2011.02025.x

51 Zhu Y, Zhou J, Ji Y, Yu B (2014) Elevated expression of AKT2 correlates with disease severity and poor prognosis in human osteosarcoma. Molecular medicine reports 10 (2):737-742. doi:10.3892/mmr.2014.2314

52 Darnell JC, Klann E (2013) The translation of translational control by FMRP: therapeutic targets for FXS. Nat Neurosci 16 (11):1530-1536. doi:10.1038/nn.3379

53 Dahlhaus R (2018) Of Men and Mice: Modeling the Fragile X Syndrome. Frontiers in molecular neuroscience 11:41. doi:10.3389/fnmol.2018.00041

54 Yu H, Lim Hong H, Tjokro Natalia O, Sathiyanathan P, Natarajan S, Chew Tian W, Klonisch T, Goodman Steven D, Surana U, Dröge P Chaperoning HMGA2 Protein Protects Stalled Replication Forks in Stem and Cancer Cells. Cell Reports 6 (4):684-697. doi:10.1016/j.celrep.2014.01.014

55 Dittmer J (2003) The Biology of the Ets1 Proto-Oncogene. Molecular Cancer 2:29-29. doi:10.1186/1476-4598-2-29

892 56 Cornils H, Kohler RS, Hergovich A, Hemmings BA (2011) Human NDR Kinases
893 Control G(1)/S Cell Cycle Transition by Directly Regulating p21 Stability. Molecular and
894 Cellular Biology 31 (7):1382-1395. doi:10.1128/MCB.01216-10
895 57 Grant TJ, Mehta AK, Gupta A, Sharif AAD, Arora KS, Deshpande V, Ting DT,
896 Bardeesy N, Ganem NJ, Hergovich A, Singh A (2017) STK38L kinase ablation promotes loss
897 of cell viability in a subset of KRAS-dependent pancreatic cancer cell lines. Oncotarget 8
898 (45):78556-78572. doi:10.18632/oncotarget.20833
899 58 Tian H, Hou L, Xiong Y-M, Huang J-X, Zhang W-H, Pan Y-Y, Song X-R (2016) miR-
900 132 targeting E2F5 suppresses cell proliferation, invasion, migration in ovarian cancer cells.
901 American Journal of Translational Research 8 (3):1492-1501
902 59 Wabitsch M, Brenner RE, Melzner I, Braun M, Moller P, Heinze E, Debatin KM,
903 Hauner H (2001) Characterization of a human preadipocyte cell strain with high capacity for
904 adipose differentiation. International journal of obesity and related metabolic disorders :
905 journal of the International Association for the Study of Obesity 25 (1):8-15
906 60 Fischer S, Wagner A, Kos A, Aschrafi A, Handrick R, Hannemann J, Otte K (2013)
907 Breaking limitations of complex culture media: functional non-viral miRNA delivery into
908 pharmaceutical production cell lines. J Biotechnol 168 (4):589-600.
909 doi:10.1016/j.jbiotec.2013.08.027
910 61 Flum M, Kleemann M, Schneider H, Weis B, Fischer S, Handrick R, Otte K (2017)
911 miR-217-5p induces apoptosis by directly targeting PRKCI, BAG3, ITGAV and MAPK1 in
912 colorectal cancer cells. Journal of cell communication and signaling. doi:10.1007/s12079-
913 017-0410-x
914 62 Rudner J, Ruiner CE, Handrick R, Eibl HJ, Belka C, Jendrossek V (2010) The Akt-
915 inhibitor Erufosine induces apoptotic cell death in prostate cancer cells and increases the
916 short term effects of ionizing radiation. Radiat Oncol 5:108. doi:10.1186/1748-717X-5-108
917 63 Cancer Genome Atlas Research N (2011) Integrated genomic analyses of ovarian
918 carcinoma. Nature 474 (7353):609-615. doi:10.1038/nature10166

64 Emmerling VV, Fischer S, Stiefel F, Holzmann K, Handrick R, Hesse F, Horer M, Kochanek S, Otte K (2016) Temperature-sensitive miR-483 is a conserved regulator of recombinant protein and viral vector production in mammalian cells. Biotechnol Bioeng 113 (4):830-841. doi:10.1002/bit.25853

65 Miranda KC, Huynh T, Tay Y, Ang YS, Tam WL, Thomson AM, Lim B, Rigoutsos I (2006) A pattern-based method for the identification of MicroRNA binding sites and their corresponding heteroduplexes. Cell 126 (6):1203-1217. doi:10.1016/j.cell.2006.07.031

66 Vlachos IS, Paraskevopoulou MD, Karagkouni D, Georgakilas G, Vergoulis T, Kanellos I, Anastasopoulos IL, Maniou S, Karathanou K, Kalfakakou D, Fevgas A, Dalamagas T, Hatzigeorgiou AG (2015) DIANA-TarBase v7.0: indexing more than half a million experimentally supported miRNA:mRNA interactions. Nucleic Acids Res 43 (Database issue):D153-159. doi:10.1093/nar/gku1215

67 Wong N, Wang X (2015) miRDB: an online resource for microRNA target prediction and functional annotations. Nucleic Acids Res 43 (Database issue):D146-152. doi:10.1093/nar/gku1104

68 Dweep H, Sticht C, Pandey P, Gretz N (2011) miRWalk--database: prediction of possible miRNA binding sites by "walking" the genes of three genomes. Journal of biomedical informatics 44 (5):839-847. doi:10.1016/j.jbi.2011.05.002

69 Thomas PD, Campbell MJ, Kejariwal A, Mi H, Karlak B, Daverman R, Diemer K, Muruganujan A, Narechania A (2003) PANTHER: a library of protein families and subfamilies indexed by function. Genome Res 13 (9):2129-2141. doi:10.1101/gr.772403

70 Chou CH, Chang NW, Shrestha S, Hsu SD, Lin YL, Lee WH, Yang CD, Hong HC, Wei TY, Tu SJ, Tsai TR, Ho SY, Jian TY, Wu HY, Chen PR, Lin NC, Huang HT, Yang TL, Pai CY, Tai CS, Chen WL, Huang CY, Liu CC, Weng SL, Liao KW, Hsu WL, Huang HD (2016) miRTarBase 2016: updates to the experimentally validated miRNA-target interactions database. Nucleic Acids Res 44 (D1):D239-247. doi:10.1093/nar/gkv1258

71 Team RC (2015) R: A language and environment for statistical computing. https://www.R-project.org/.

947 72 Livak KJ, Schmittgen TD (2001) Analysis of relative gene expression data using real-
948 time quantitative PCR and the 2(-Delta Delta C(T)) Method. Methods 25 (4):402-408.
949 doi:10.1006/meth.2001.1262

950

Figure Legends

Figure 1 MiRNA screen validation and miR-493 expression in ovarian cell lines

For validation screening T98G, HCT 116, SKOV3, and SGBS cells were seeded 24 h before transfection with miRNA mimics (50 nM and 0.4 µl ScreenFect A) or non-targeting siRNA (NT, negative control for cell death) control. Apoptosis rates 72 h after transfection were analysed by Nicoletti staining followed by flow cytometric analysis (a). The location of miRNA-493 is in chromosome 14 in a miRNA cluster between Meg3 and RTL1 (b). QRT-PCR of untreated ovarian cells for miR-493-3p and -5p expression (c). For determination of miR-493 expression after induction of apoptosis, SKOV3 (d) and OVCAR3 (e) cells were seeded in 24 h prior treatment with 25 µM Etoposide, 80 µM Carboplatin or 0.25 µM Paclitaxel for additional 48 h. The miRNA expression of miR-493 was normalized to the CT value of U6 snRNA and the untreated control (d, e) or the expression in HOSE 2170 cells (c) employing the Livak method [72]. Statistical analyses were performed by one-way ANOVA (a, d, e) followed by Bonferroni post-test. For part (c) an unpaired t test was used [n = 3 replicates; mean ± SD, *$p < 0.05$; **$p < 0.01$; ***$p < 0.001$; ****$p < 0.0001$].

Figure 2 Analysis of apoptosis induction by miR-493

The ovarian CA cell lines SKOV3, OVCAR3, TOV21G, TOV112D, A2780 as well as A2780-cis were seeded 24 h prior transfection with 62.5 nM miR-493 mimics, non-targeting siRNA (NT, negative control for cell death), cell death inducing siRNA (DT, positive control for cell death) or treatment with 25 µM Etoposide, 80 µM Carboplatin or 0.25 µM Paclitaxel in 96 well plates. 48 h after treatment the cells were analysed for their release of cytochrome C (b) as well as the loss of $\Delta\Psi m$ (c). 72 h after treatment the cell confluency (a) and the fragmentation of DNA (d) was analysed. 5 µM CCCP served as a positive control for the breakdown of $\Delta\Psi m$ (c). Statistical

977 analysis was performed by one-way ANOVA followed by Bonferroni post-test. [n = 3
978 replicates; mean ± SD, *p < 0.05; **p < 0.01; ***p < 0.001; ****p < 0.0001]
979
980 **Figure 3 Activation of caspase 3/ -7 by miR-493**
981 For long term analysis SKOV3 cells were seeded and transfected as described in
982 Figure 2. To detect apoptosis induction by miR-493 the cells were stained with
983 IncuCyte AnnexinV Red Reagent (a) or IncuCyte Caspase-3/7 Green Apoptosis
984 Assay Reagent (b). The cells were automatically photographed every hour by the
985 IncuCyte ZOOM System. The amount of AnnexinV positive cells or cells with
986 activated caspase 3 or -7 were calculated by the IncuCyte ZOOM Software. For
987 Western Blot analysis the cells were harvested 72 h after treatment. ß-Actin served
988 as a loading control. Cells were treated with 30 µM zVAD to inhibit caspase 3 activity
989 (c). For measuring motility, cells were seeded, scratched with a 1000 µl pipet tip and
990 transfected with the negative control siRNA (NT), miR-493 or the cell death positive
991 control (DT). 0 h and 24 h after transfection images of the cell layer were taken by the
992 automated single well microscope NyOne (d). The distance of the gap was measured
993 and plotted on a box-and-whisker diagram (e). Statistical analyses were performed
994 by one-way ANOVA followed by Bonferroni post-test. [n = 3 replicates; mean ± SD,
995 *p< 0.05, **p< 0.01, ***p < 0.001, ****p < 0.0001]
996
997 **Figure 4 Post-transcriptional regulations of miR-493 target genes**
998 To validate miR-493 mediated regulation of potential target genes, SKOV3 and
999 OVCAR3 cells were transfected with miR-493 mimic or non-targeting siRNA (NT) as
1000 described in Figure 2. After 48 h, potential target gene expression was analysed by
1001 qRT-PCR. The relative mRNA expression of potential target genes was normalized to
1002 PPIA and NT (a) employing the Livak method [72]. The significance was determined

using unpaired t-test. Significantly downregulated potential targets were further analysed by Western Blotting (b). GAPDH was used as loading control. Downregulated potential targets were further analysed by Luciferase Reporter Assay (c, d) to proof direct binding of the miRNA to its predicted target sequence. Anti-miR-493 was used to confirm the binding sites of miR-493 to the target mRNAs (c). The binding sites in the 3' UTR with (c) and without seed sequence (d, Table 2), based on data of microRNA.org [35] and TargetScanHuman [34], were cloned into a pMirGLO vector. Relative luciferase activity was measured 72 h after co-transfection of the pMirGLO vector with miR-493 mimic, miRNA inhibitor anti-miR-493 or non-targeting siRNA (NT) in HEK293T cells. The relative luciferase expression was normalized to the expression after co-transfection with NT. The significance was determined using unpaired t-test. [n = 3 replicates; mean ± SD, *p< 0.05, **p< 0.01, ***p < 0.001, ****p < 0.0001]

Figure 5 Downstream signalling induced by miR-493-3p

To detect the apoptosis signalling pathway after transfection of miR-493 leading to apoptosis Western Blotting were conducted (a). ß-Actin served as a loading control. Kaplan-Meier Blots of old (older than 67.5 years) ovarian serous cystadenocarcinoma patients (data from TCGA) with a low and high expression (mean cut-off) of AKT2 (b) or STK38L (c) were performed to demonstrate median survival. Prolonged survival time of ovarian CA patients expressing low levels (blue) of AKT2 or STK38L compared to high expressers (red line).

Figure 6 Transcriptome analysis detecting regulated transcription factors

To validate the results of the transcriptome analysis (Table 3) a qRT-PCR was carried out to analyse the expression of ETS1 and ETS2, E2F5 and QKI. The cells

1029 were transfected with miR-493 mimic or non-targeting siRNA (NT) as described in
1030 Figure 2. The relative mRNA expression of potential target genes was normalized to
1031 PPIA and NT (a and e) employing the Livak method [72]. The significance was
1032 determined using unpaired t-test. The transcription factors were further analysed by
1033 Western Blotting (b). GAPDH was used as loading control. To proof direct binding of
1034 the miRNA to its predicted target sequence luciferase assays were performed as
1035 described in Figure 4. The binding sites in the 3' UTR with (c) and without seed
1036 sequence (d, Table 2), based on data of microRNA.org [35] and TargetScanHuman
1037 [34], were cloned into a pMirGLO vector. Anti-miR-493 was used to confirm the
1038 binding sites of miR-493 to the target mRNAs (c). The relative luciferase expression
1039 was normalized to the expression after co-transfection with NT. The significance was
1040 determined using unpaired t-test. To demonstrate the influence of ETS1 as
1041 transcription factor of RAF1 a qRT-PCR was performed with miRNA-493, NT and
1042 siRNA transfected cells (e).Further,transfected cell lysates were used for Western
1043 Blotting to observe effects on protein level. GAPDH served as loading control (f).
1044 Additionally, the fragmentation of DNA was measured by Nicoletti assay 72 h after
1045 transfection (g). Statistical analysis was performed by one-way ANOVA followed by
1046 Bonferroni post-test. [n = 3 replicates; mean ± SD, *p< 0.05, **p< 0.01, ***p < 0.001,
1047 ****p < 0.0001]
1048
1049 **Figure 7 STK38L is phosphorylating RAF1**
1050 To demonstrate an interaction of STK38L with RAF1 immunoprecipitations were
1051 carried out.. Protein lysates of SKOV3 cells were precipitated for RAF1 or STK38L
1052 and blotted against both proteins (a). To obtain more information about the
1053 interaction between STK38L and RAF1, HEK293T cells were transfected with
1054 overexpression plasmids of Flag tagged STK38L Wild Type (Flag-STK38L WT) or a

kinase dead version of STK38L (Flag-STK38L KD). The protein lysates were precipitated for RAF1 and blotted for total RAF1 and phosphorylated RAF1 (Ser621) (b, left part). The lysates were blotted against the Flag tag to demonstrate equal STK38L overexpression (b, right part). GAPDH served as loading control. [n = 2 replicates] The regulation of RAF1 by STK38L and ETS1 is illustrated schematically in part d. Furthermore, the signalling pathways leading to apoptosis in ovarian CA cell lines is shown schematically in part c.

Supplementary Figure 1 Determination of miR-493 expression after transfection For determination of miR-493 expression after transfection, cells were seeded and transfected as described in Figure 2. The miRNA expression of miR-493 was normalized to the CT value of U6 snRNA and the NT transfected control employing the Livak method [72]. Statistical significance was tested by an unpaired t test. [n = 3 replicates; mean ± SD, *p < 0.05; **p < 0.01; ***p < 0.001; ****p < 0.0001]

Tables

Table 1 putative miRNA-493 target genes clustered by the IPA analysis or by miRNA correlation to potential targets on mRNA and protein level of the TCGA ovarian serous cystadenocarcinoma dataset

Potential target	Gene name	Cluster function	Correlation coefficient	P-value
STAT3	Signal Transducer And Activator Of Transcription 3	IPA analysis: ovarian CA signalling	-	-
HMGA2	High Mobility Group AT-Hook 2	IPA analysis: ovarian CA signalling	-	-
MAP2K5	Mitogen-Activated Protein Kinase Kinase 5	IPA analysis: ovarian CA signalling	-	-
AKT2	AKT Serine/Threonine Kinase 2	IPA analysis: ovarian CA signalling	-	-
PEA15	Phosphoprotein Enriched In Astrocytes 15	TCGA analysis, correlation to mRNA expression	-0.16034	0.00198
ALKBH3	AlkB Homolog 3, Alpha-Ketoglutaratedependent Dioxygenase	TCGA analysis, correlation to mRNA expression	-0.14968	0.00391
FMR1P	Fragile X Mental Retardation 1	TCGA analysis, correlation to mRNA expression	-0.12411	0.01692
PIK3R3	Phosphoinositide-3-Kinase Regulatory Subunit 3	TCGA analysis, correlation to mRNA expression	-0.10594	0.04168
STK38L	Serine/Threonine Kinase 38 Like	TCGA analysis, correlation to mRNA expression	-0.09455	0.06929

EEF2K	Eukaryotic Elongation Factor 2 Kinase	TCGA analysis, correlation to protein expression	-0.25752	0.00003
FOXM1	Forkhead Box M1	TCGA analysis, correlation to protein expression	-0.18188	0.00350
JAK2	Janus Kinase 2	TCGA analysis, correlation to protein expression	-0.17445	0.00512
ADAR1	Adenosine Deaminase, RNA Specific	TCGA analysis, correlation to protein expression	-0.17357	0.00536
GAB2	GRB2 Associated Binding Protein 2	TCGA analysis, correlation to protein expression	-0.16114	0.00981
RAF1	Raf-1 Proto-Oncogene, Serine/Threonine Kinase	TCGA analysis, correlation to protein expression	-0.16050	0.01011
MAPK1	Mitogen-Activated Protein Kinase 1	TCGA analysis, correlation to protein expression	-0.13321	0.03314

Table 2 predicted binding sites cloned into a pmirGlo Dual Luciferase miRNA target expression vector

Target mRNA_nr. of binding site	Localication in 3' UTR (nt)	Binding sequence	
AKT2	2955-2978	5' cugGGCAuCAUAgGgAGACCUUCa 3'	AKT2
		3' ggaCCGU-GUGU-CaUCUGGAAGu 5'	hsa-miR-493-3p
HMGA2_1	175-197	5' aggacuauauuuaaucACCUUCu 3'	HMGA2
		3' ggaccgugugucaucUGGAAGu 5'	hsa-miR-493-3p
HMGA2_2	1855-1877	5' auaaaauaAaAGccaACCUUCAa 3'	HMGA2
		3' ggaccgugUgUCaucUGGAAGU 5'	hsa-miR-493-3p
STK38L_1	655-681	5' aggaagACAaAGUuuaAcACCUUCAc 3'	STK38L
		3' ggaccgUGUgUCA---UcUGGAAGU 5'	hsa-miR-493-3p
STK38L_2	709-731	5' uucagaaAUACuGauGACCUUCA 3'	STK38L
		3' ggaccgUGUGuCauCUGGAAGU 5'	hsa-miR-493-3p
FOXM1	290-311	5' gcccagcagucucuuACCUUCc 3'	FOXM1
		3' ggaccgugugucaucUGGAAGu 5'	hsa-miR-493-3p
RAF1	105-127	5' gaagcUGcUGCuaAG--GACCUUCu 3'	RAF1
		3' ggACcGUGugUCauCUGGAAGu 5'	hsa-miR-493-3p
FMR1P	1267-1289	5' gaaaaaUAUGUGaaGGACCUUCa 3'	FMR1P
		3' ggaccGUGUGUcaUCUGGAAGu 5'	hsa-miR-493-3p
ETS1_1	20-41	5' gaaacCCUGCUG-AGACCUUCc 3'	ETS1
		3' ggaccGUGUGUCAUCUGGAAGu 5'	hsa-miR-493-3p
ETS1_2	100-122	5' cagaacucauuuuuuACCUUCa 3'	ETS1
		3' ggaccgugugucaucUGGAAGu 5'	hsa-miR-493-3p
ETS1_3	2993-3015	5' gcauuaaccugccuaACCUUCa 3'	ETS1
		3' ggaccgugugucaucUGGAAGu 5'	hsa-miR-493-3p
ETS2	1711-1734	5' caauaCCCACAAAAGACCAUUCc 3'	ETS2
		3' ggaccGUGUGUCAUCUGG-AAGu 5'	hsa-miR-493-3p
E2F5	1629-1651	5' cugaauccuuccUGGACCUUCu 3'	E2F5
		3' ggaccgugugucAUCUGGAAGu 5'	hsa-miR-493-3p

1081 **Table 3 putative miRNA-493 target genes of gene expression analysis**

Potential target	Gene name	Fold change	Nr. of pred. binding sites	Publication with potential target and RAF1
ETS1	ETS proto-oncogene 1	0.41586	3	
PER3	period circadian clock 3	0.68510	3	
LITAF	lipopolysaccharide-induced TNF factor	0.72157	3	
BRPF3	bromodomain and PHD finger containing 3	0.73974	2	
E2F5	E2F transcription factor 5	0.75320	1	[38] and [39]
SP100	SP100 nuclear antigen	0.75919	1	
SSX9	SSX family member 9	0.76158	1	
ZNF778	Zinc finger protein 778	0.77051	1	
NFATC3	nuclear factor of activated T cells 3	0.77707	1	
ETS2	ETS proto-oncogene 1	0.78407	1	[40]
HOXC11	homeobox C11	0.79009	2	
QKI	QKI, KH domain containing RNA binding	0.79066	4	[41]

1082

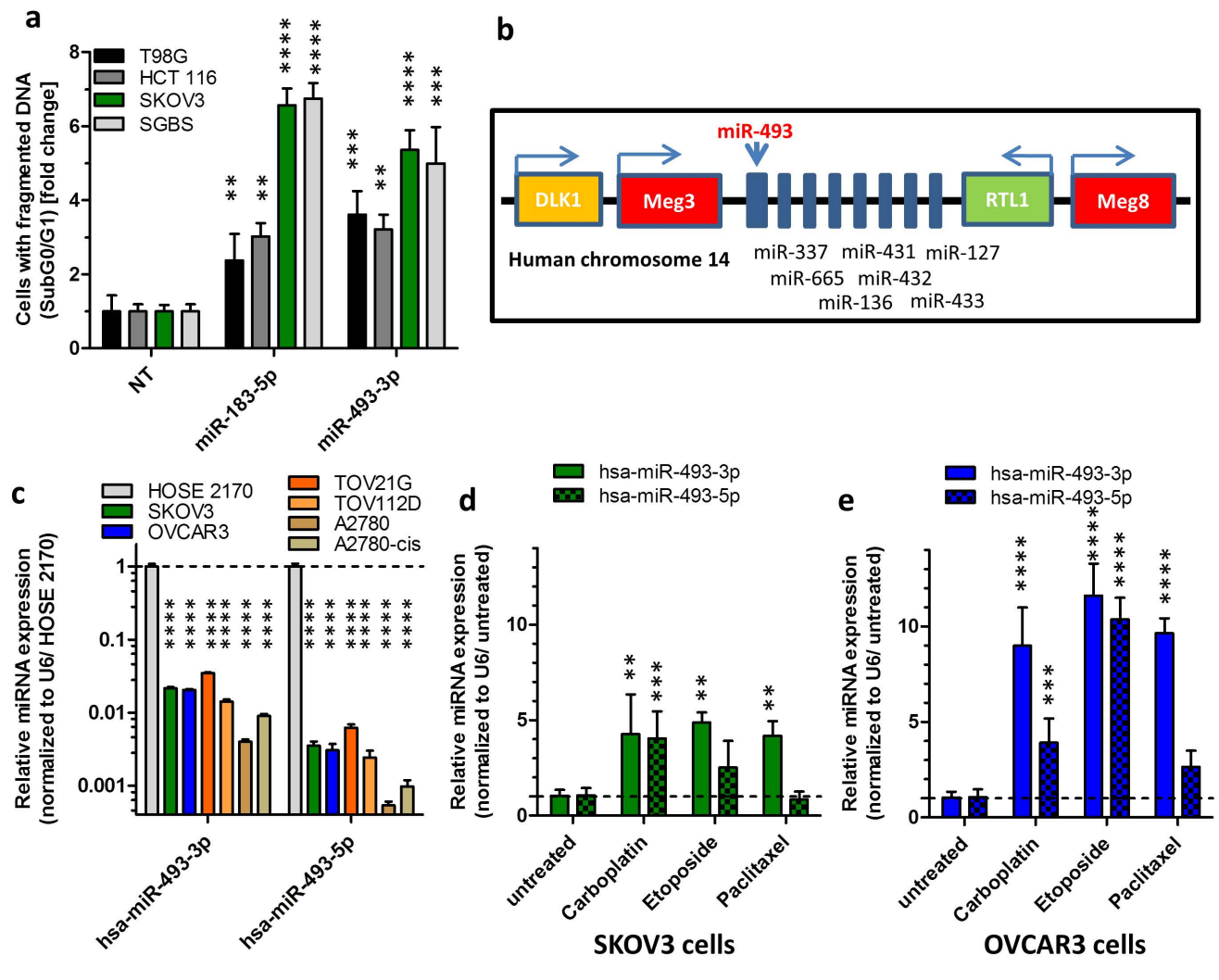
a
Cells with fragmented DNA (SubG0/G1) [fold change]
T98G
HCT 116
SKOV3
SGBS
NT
miR-183-5p
miR-493-3p
b
miR-493
DLK1
Meg3
RTL1
Meg8
Human chromosome 14
miR-337 miR-431 miR-127
miR-665 miR-432
miR-136 miR-433
c
Relative miRNA expression (normalized to U6/ HOSE 2170)
HOSE 2170
SKOV3
OVCAR3
TOV21G
TOV112D
A2780
A2780-cis
hsa-miR-493-3p
hsa-miR-493-5p
d
Relative miRNA expression (normalized to U6/ untreated)
hsa-miR-493-3p
hsa-miR-493-5p
untreated
Carboplatin
Etoposide
Paclitaxel
SKOV3 cells
e
Relative miRNA expression (normalized to U6/ untreated)
hsa-miR-493-3p
hsa-miR-493-5p
untreated
Carboplatin
Etoposide
Paclitaxel
OVCAR3 cells

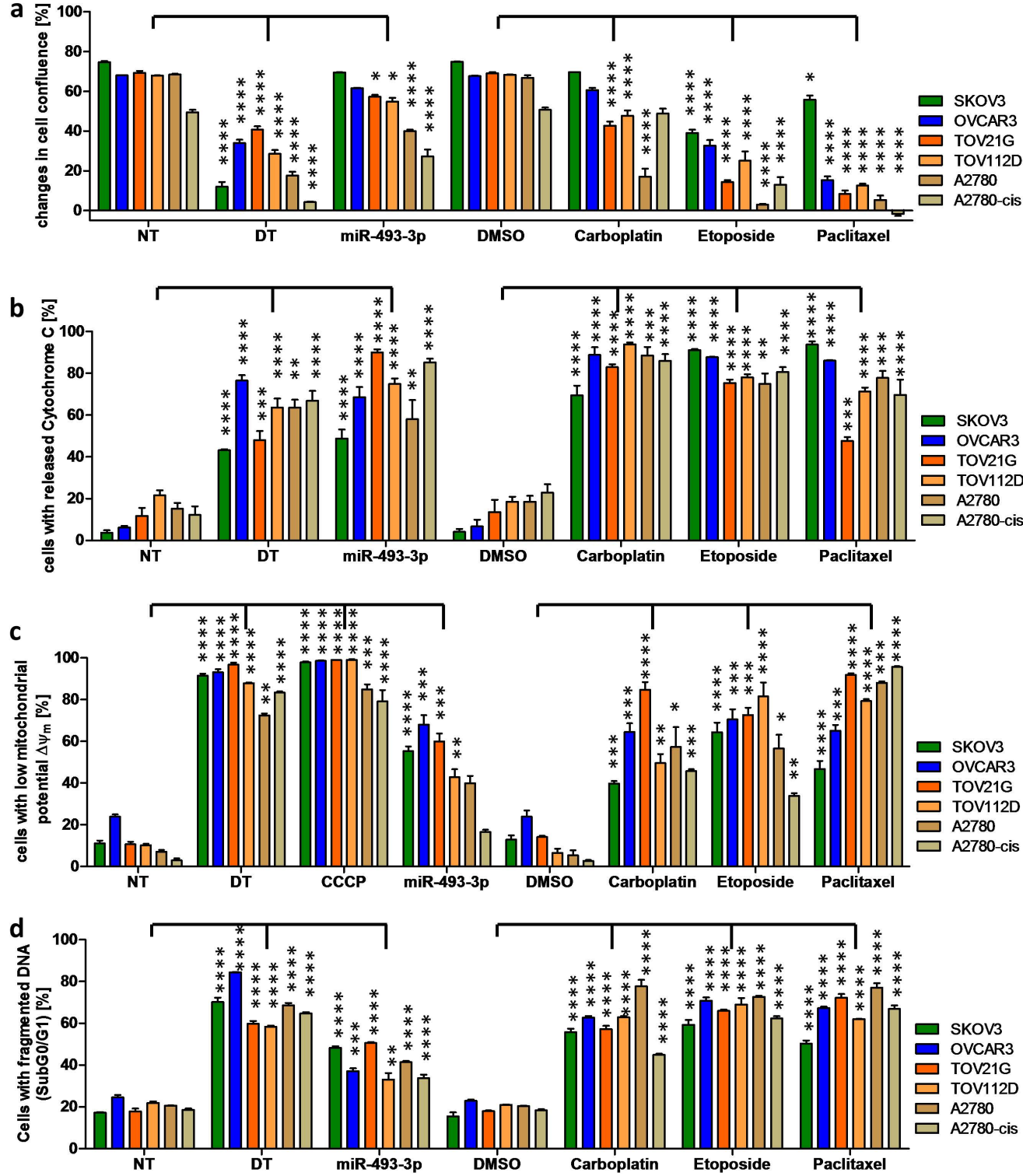
a
changes in cell confluence [%]
100
80
60
40
20
0
NT
DT
miR-493-3p
DMSO
Carboplatin
Etoposide
Paclitaxel
SKOV3
OVCAR3
TOV21G
TOV112D
A2780
A2780-cis
b
cells with released Cytochrome C [%]
100
80
60
40
20
0
NT
DT
miR-493-3p
DMSO
Carboplatin
Etoposide
Paclitaxel
SKOV3
OVCAR3
TOV21G
TOV112D
A2780
A2780-cis
c
cells with low mitochondrial potential Δψm [%]
100
80
60
40
20
0
NT
DT
CCCP
miR-493-3p
DMSO
Carboplatin
Etoposide
Paclitaxel
SKOV3
OVCAR3
TOV21G
TOV112D
A2780
A2780-cis
d
Cells with fragmented DNA (SubG0/G1) [%]
100
80
60
40
20
0
NT
DT
miR-493-3p
DMSO
Carboplatin
Etoposide
Paclitaxel
SKOV3
OVCAR3
TOV21G
TOV112D
A2780
A2780-cis

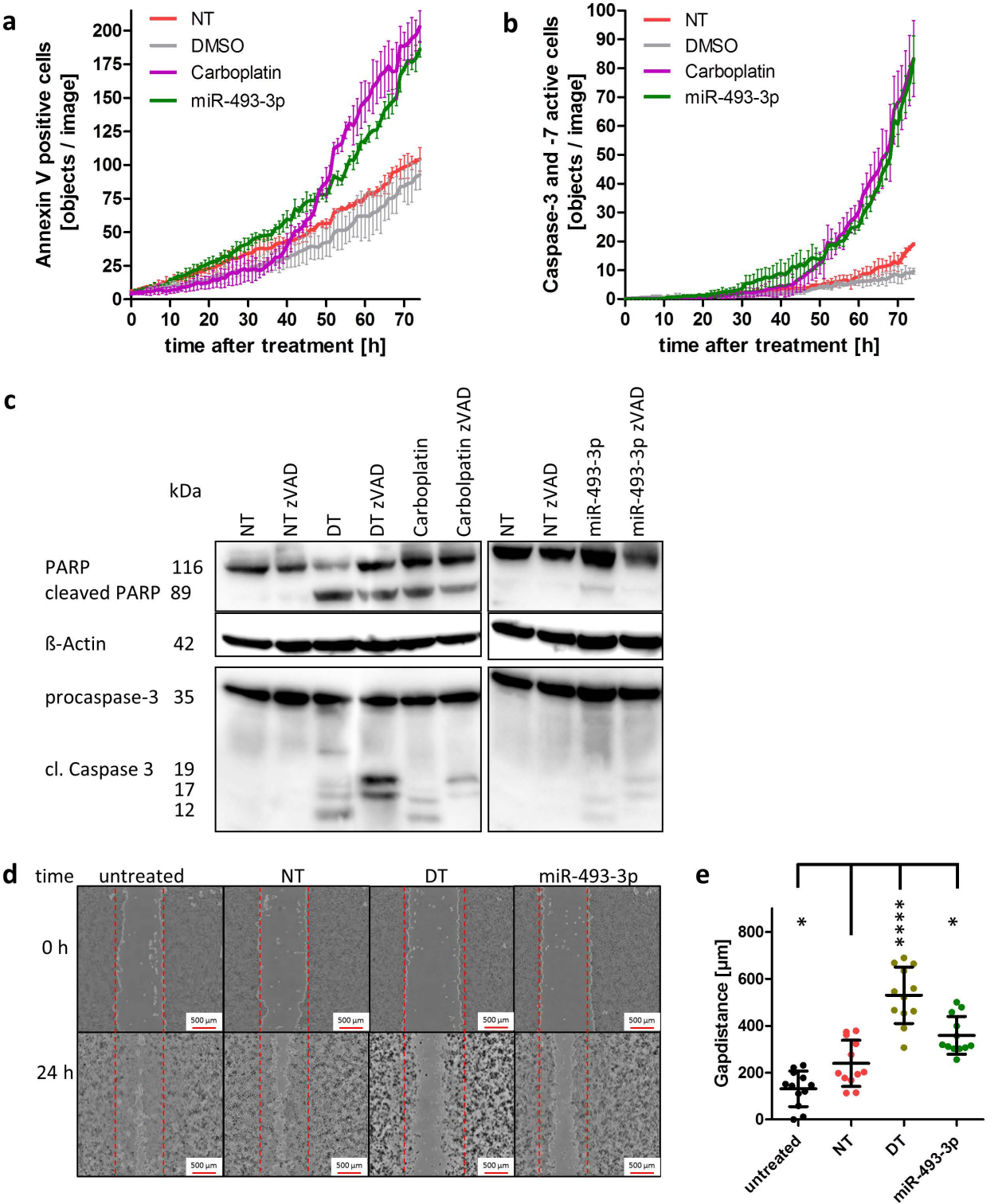
a
Annexin V positive cells [objects / image]
NT
DMSO
Carboplatin
miR-493-3p
time after treatment [h]
b
Caspase-3 and -7 active cells [objects / image]
NT
DMSO
Carboplatin
miR-493-3p
time after treatment [h]
c
kDa
NT
NT zVAD
DT
DT zVAD
Carboplatin
Carbolpatin zVAD
NT
NT zVAD
miR-493-3p
miR-493-3p zVAD
PARP 116
cleaved PARP 89
ß-Actin 42
procaspase-3 35
cl. Caspase 3 19
17
12
d
time
untreated
NT
DT
miR-493-3p
0 h
24 h
500 µm
e
Gapdistance [µm]
untreated
NT
DT
miR-493-3p

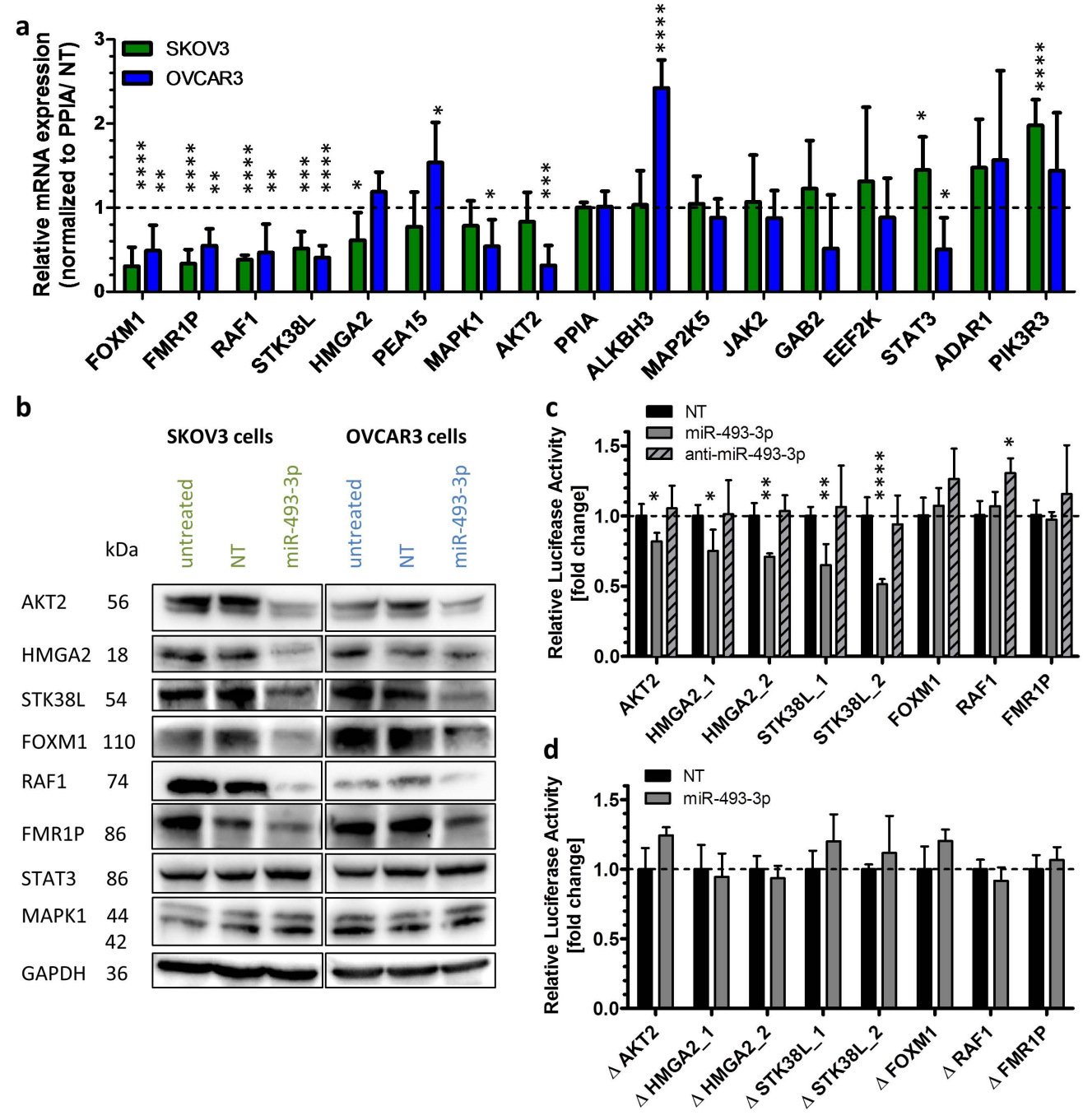
a
Relative mRNA expression (normalized to PPIA/ NT)
SKOV3
OVCAR3
FOXM1
FMR1P
RAF1
STK38L
HMGA2
PEA15
MAPK1
AKT2
PPIA
ALKBH3
MAP2K5
JAK2
GAB2
EEF2K
STAT3
ADAR1
PIK3R3
b
SKOV3 cells
OVCAR3 cells
untreated
NT
miR-493-3p
kDa
AKT2 56
HMGA2 18
STK38L 54
FOXM1 110
RAF1 74
FMR1P 86
STAT3 86
MAPK1 44 42
GAPDH 36
c
NT
miR-493-3p
anti-miR-493-3p
Relative Luciferase Activity [fold change]
AKT2
HMGA2_1
HMGA2_2
STK38L_1
STK38L_2
FOXM1
RAF1
FMR1P
d
NT
miR-493-3p
Relative Luciferase Activity [fold change]
Δ AKT2
Δ HMGA2_1
Δ HMGA2_2
Δ STK38L_1
Δ STK38L_2
Δ FOXM1
Δ RAF1
Δ FMR1P

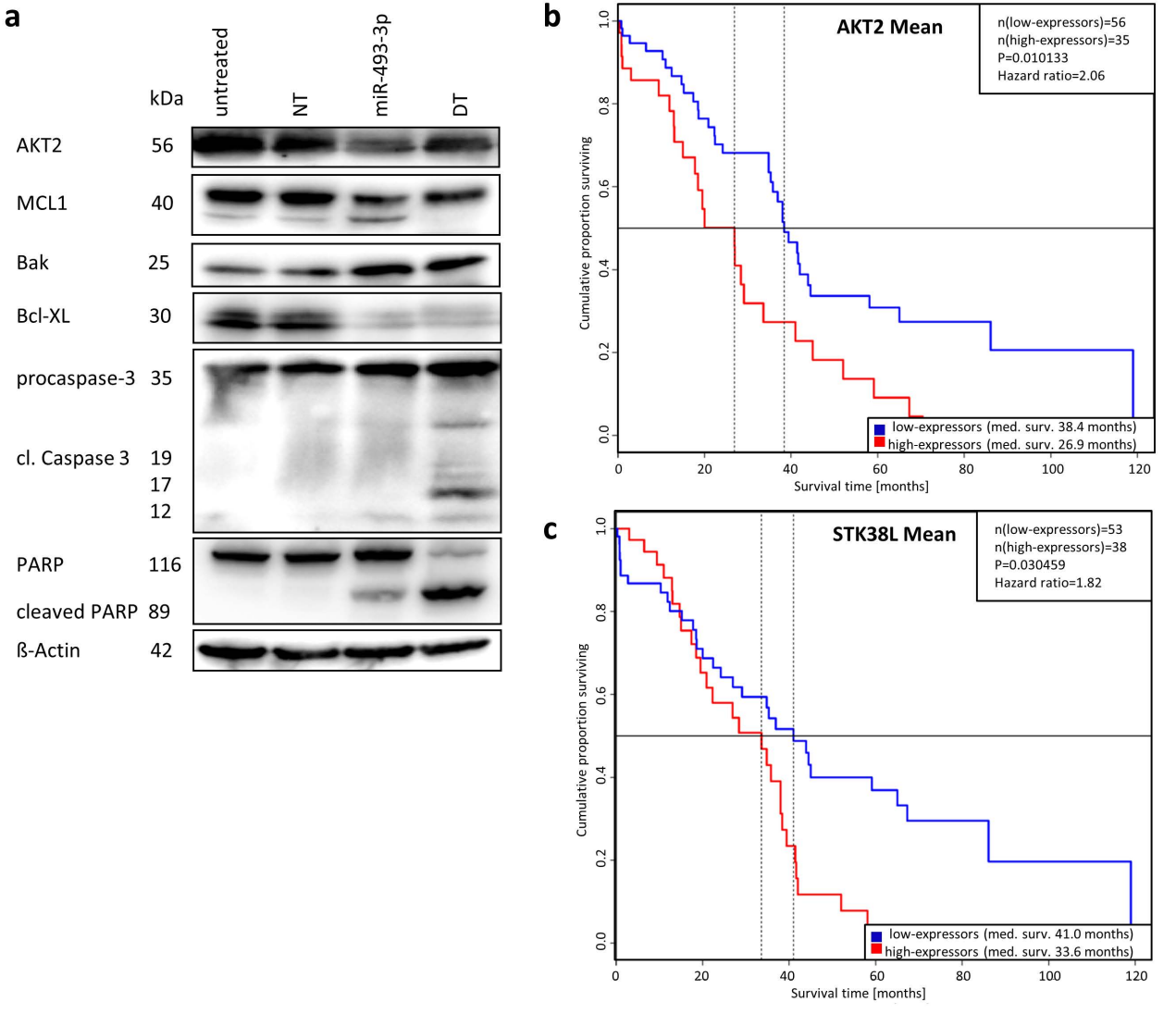
a
kDa
untreated
NT
miR-493-3p
DT
AKT2
56
MCL1
40
Bak
25
Bcl-XL
30
procaspase-3
35
cl. Caspase 3
19
17
12
PARP
116
cleaved PARP
89
ß-Actin
42
b
AKT2 Mean
n(low-expressors)=56
n(high-expressors)=35
P=0.010133
Hazard ratio=2.06
Cumulative proportion surviving
low-expressors (med. surv. 38.4 months)
high-expressors (med. surv. 26.9 months)
Survival time [months]
c
STK38L Mean
n(low-expressors)=53
n(high-expressors)=38
P=0.030459
Hazard ratio=1.82
Cumulative proportion surviving
low-expressors (med. surv. 41.0 months)
high-expressors (med. surv. 33.6 months)
Survival time [months]

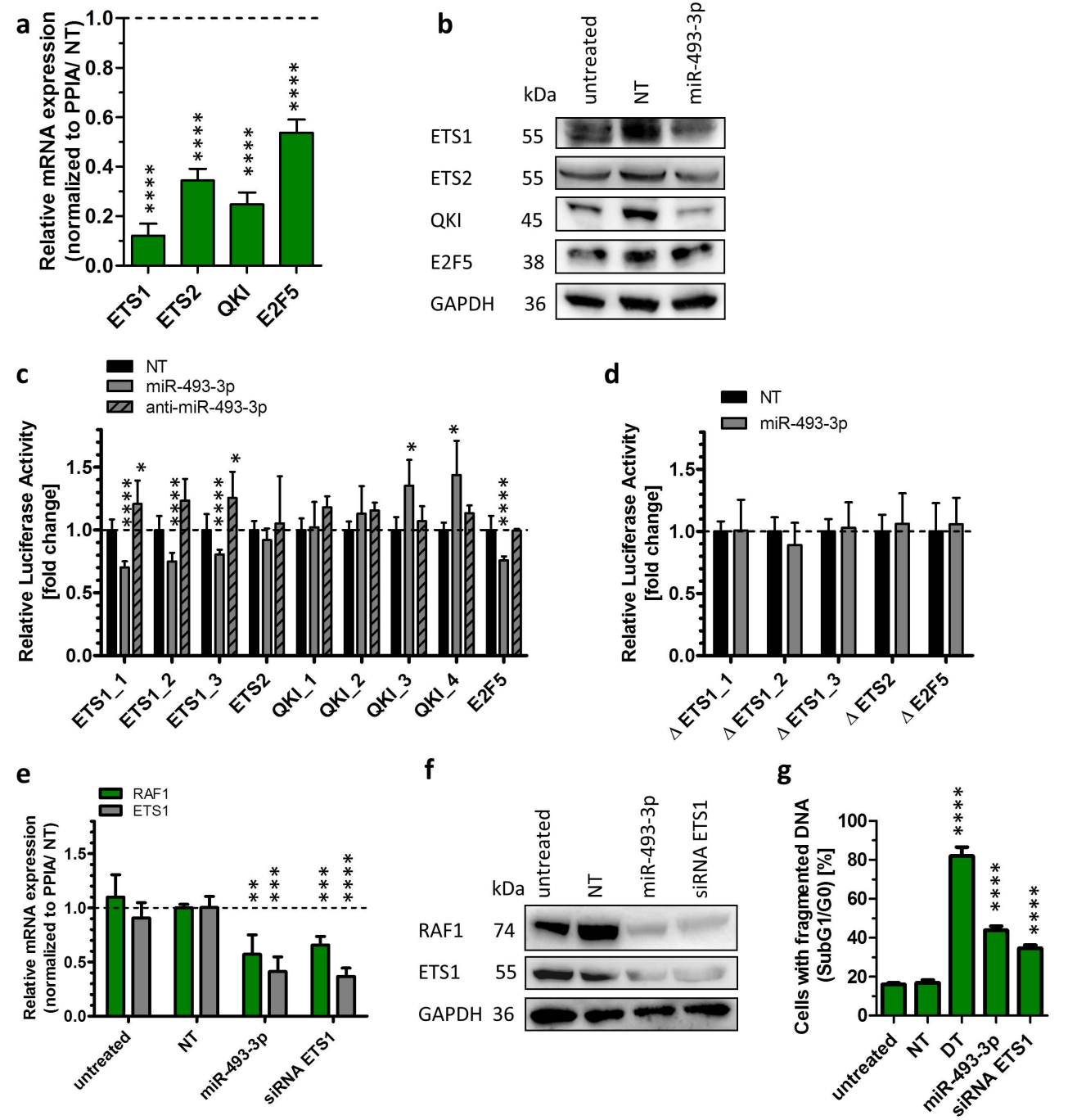
a
Relative mRNA expression (normalized to PPIA/ NT)
1.0
0.8
0.6
0.4
0.2
0.0
****
****
****
****
ETS1
ETS2
QKI
E2F5
b
kDa
untreated
NT
miR-493-3p
ETS1 55
ETS2 55
QKI 45
E2F5 38
GAPDH 36
c
NT
miR-493-3p
anti-miR-493-3p
Relative Luciferase Activity [fold change]
1.5
1.0
0.5
0.0
ETS1_1
ETS1_2
ETS1_3
ETS2
QKI_1
QKI_2
QKI_3
QKI_4
E2F5
d
NT
miR-493-3p
Relative Luciferase Activity [fold change]
1.5
1.0
0.5
0.0
Δ ETS1_1
Δ ETS1_2
Δ ETS1_3
Δ ETS2
Δ E2F5
e
RAF1
ETS1
Relative mRNA expression (normalized to PPIA/ NT)
1.5
1.0
0.5
0.0
untreated
NT
miR-493-3p
siRNA ETS1
f
kDa
untreated
NT
miR-493-3p
siRNA ETS1
RAF1 74
ETS1 55
GAPDH 36
g
Cells with fragmented DNA (SubG1/G0) [%]
100
80
60
40
20
0
****
****
****
untreated
NT
DT
miR-493-3p
siRNA ETS1

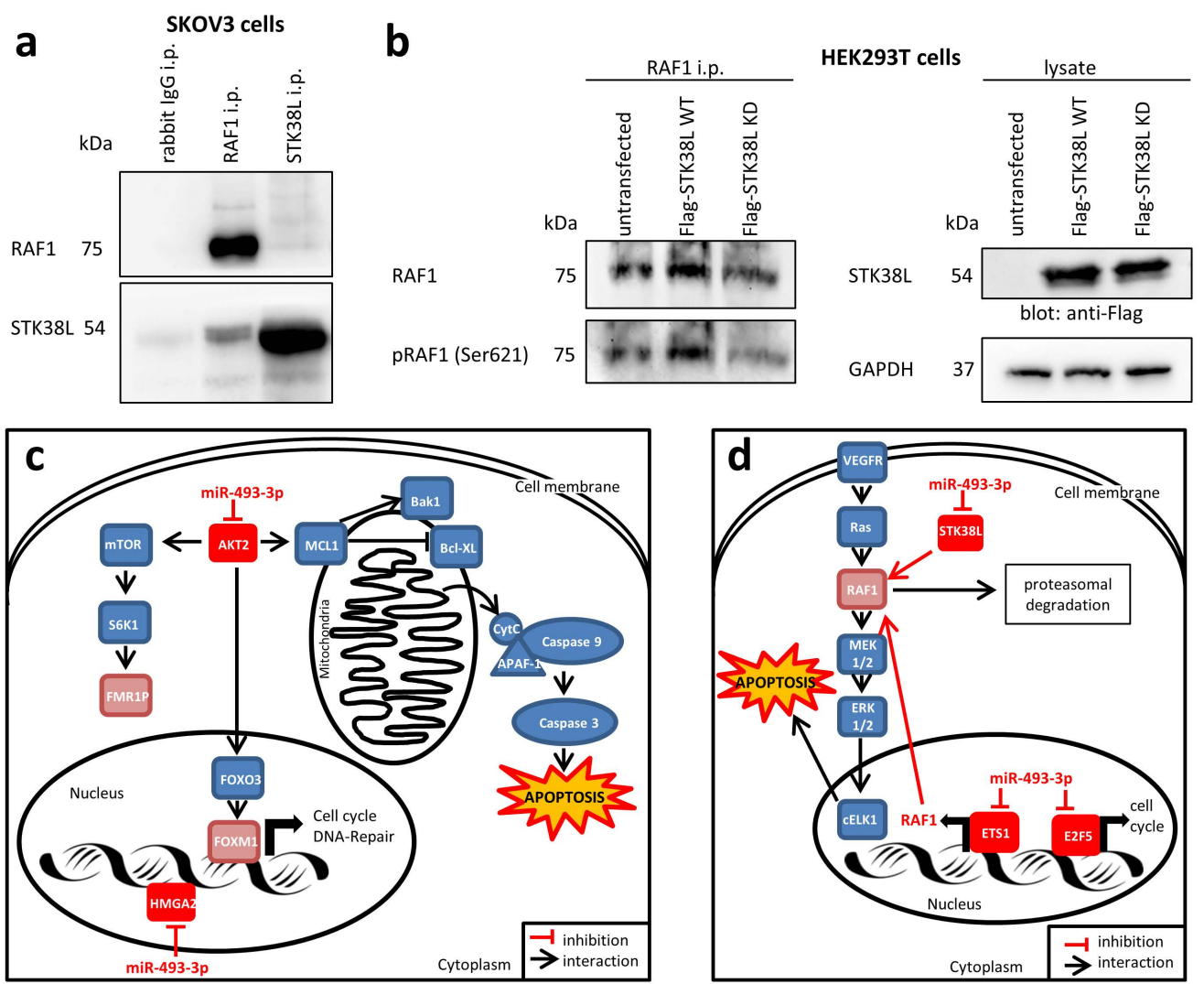
a
SKOV3 cells
rabbit IgG i.p.
RAF1 i.p.
STK38L i.p.
kDa
RAF1 75
STK38L 54
b
RAF1 i.p.
untransfected
Flag-STK38L WT
Flag-STK38L KD
kDa
RAF1 75
pRAF1 (Ser621) 75
HEK293T cells
lysate
untransfected
Flag-STK38L WT
Flag-STK38L KD
kDa
STK38L 54
blot: anti-Flag
GAPDH 37
c
Cell membrane
miR-493-3p
Bak1
AKT2
MCL1
Bcl-XL
mTOR
S6K1
FMR1P
Mitochondria
CytC
APAF-1
Caspase 9
Caspase 3
APOPTOSIS
Nucleus
FOXO3
FOXM1
Cell cycle
DNA-Repair
HMGA2
miR-493-3p
Cytoplasm
inhibition
interaction
d
VEGFR
Ras
RAF1
miR-493-3p
STK38L
Cell membrane
proteasomal
degradation
MEK
1/2
ERK
1/2
APOPTOSIS
cELK1
RAF1
miR-493-3p
ETS1
E2F5
cell
cycle
Nucleus
Cytoplasm
inhibition
interaction

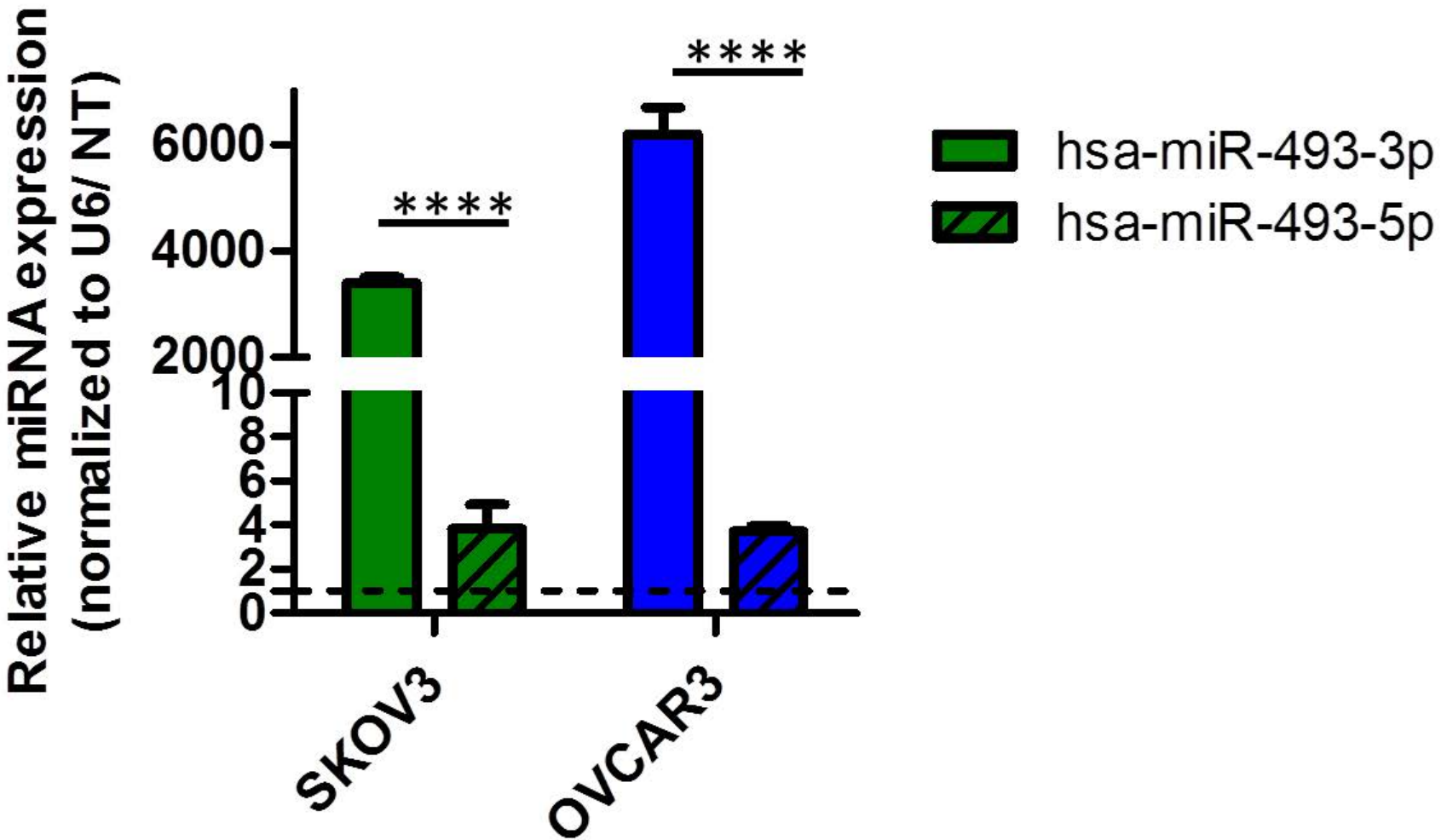
Relative miRNA expression
(normalized to U6/ NT)
6000
4000
2000
10
8
6
4
2
0
****
****
SKOV3
OVCAR3
hsa-miR-493-3p
hsa-miR-493-5p